Assessment of the Synoptic Variability of the Antarctic Marginal Ice Zone with *In Situ* Observations

Ehlke de Jong

Supervised by Associate Professor Marcello Vichi

Physical Oceanography

This dissertation is presented for the degree of

Master of Science

In the Department of Oceanography

University of Cape Town

February 2019

Soli Deo Gloria

Declaration

I know the meaning of plagiarism and declare that all the work in the document, save that which is properly acknowledged, is my own. This dissertation has been submitted to the Turnitin module and I confirm that my supervisor has seen my report and any concerns revealed by such have been resolved with my supervisor.

Signed: Signed by candidate

Date: 6 February 2019

Ehlke de Jong

Cape Town

ABSTRACT

Knowledge of sea ice variability, which contributes to the detection of climate change trends, stems primarily from remote sensing information. However, sea ice in the Southern Ocean is characterised by large variability that remains unresolved and limits our confidence on the remotely sensed products. Although one of the biggest seasonal changes on Earth is the annual advance and retreat of the Antarctic sea ice cover, relatively little attention has been given to the processes by which the marginal ice zone (MIZ) edge forms and responds to synoptic events. This study aimed to assess the seasonal sea ice extent (SIE) of the MIZ by comparing sea ice observations estimated from aboard ship to high resolution passive microwave (PM) satellite imagery when transecting the MIZ. To achieve this, sea ice concentration (SIC) was derived from two AMSR2 (Advanced Microwave Scanning Radiometer 2) products; the ARTIST (Arctic Radiation and Turbulence Interaction STudy) Sea Ice (ASI-AMSR2) and the bootstrap (BST-AMSR2). The ice concentration estimated from these PM satellite products was assessed against SIC observations collected from the *S.A. Agulhas II* (using the Antarctic Sea Ice Processes and Climate (ASPeCt) protocol). This assessment took place over summer and winter for the years 2016 and 2017. After evaluating how well these PM-SIC estimates compared against the ASPeCt SIC observations, we found that there was good correlation over summer MIZ conditions, while over winter MIZ conditions the correlation was relatively poor. This highlighted winter limitations inherent in PM SIC estimates. Therefore, from these comparison results, an analysis of the seasonal SIE was accomplished while being aware of the winter limitations linked to the PM products. We inferred that the MIZ acts as an indicator for what the evolution of winter SIE might look like over the following months. In addition to winter limitations associated with PM-SIC retrievals, the ASPeCt SIC estimates, based on human interpretation of the sea ice conditions, was limited because of subjective bias. This resulted in the development of an algorithm to automatically acquire SIC from image stills and videos. This method can be used to obtain quantitative sea ice data from vessels of opportunity without the need to have trained personnel on-board. In summary, this study assesses seasonal MIZ SIE within the Atlantic sector after highlighting the limitations associated with various SIC-retrieval methods.

ACKNOWLEDGEMENTS

For their help at various stages of my thesis, my acknowledgement and thanks are given to:

A/ Prof. Marcello Vichi for your guidance and for the opportunities to travel and continuously learn. You have allowed me to grow academically - more than I could have imagined. I look back to when you started supervising me at honours level, and you have played a significant role in my life over the years. You are continuously teaching and molding me. I cannot put a price on that.

My **mom, dad** and **sister**, for your non-stop support and for (quite literally) cheering me on always. I am incredibly grateful for the love you shower me with daily and for continuously praying for me.

James Hepworth, simply thank you!

The National Research Foundation (**NRF**) and the University of Cape Town (**UCT**) financial need programme for funding my master's degree (and my degrees before this one). I would not have been able to study without your assistance.

The Scientific Committee on Antarctic Research (**SCAR**) for contributing towards funding Trond Robertsen to teach me about observing the Antarctic sea ice environment during the 2016 winter expedition.

The Department of Environmental Affairs (**DEA**) for funding the Antarctic expeditions aboard the *S.A. Agulhas II*.

The South African National Antarctic Programme (**SANAP**) and the Captains and crew aboard the *S.A. Agulhas II* for making the Antarctic expeditions possible.

Dr. Carolin Mehlmann and her team in the Institute of Analysis and Numerics, University of Magdeburg, Germany. Thank you for the time and energy you put into helping me develop an algorithm to automatically acquire ice concentration. I would not have been able to complete such a task without your help.

Dr. Howard Waldron for taking the time to proofread my thesis and for being a wonderful support since my first Antarctic expedition in 2016. Thank you for walking this long, exciting road with me.

Trond Robertsen for showing me the world of sea ice. I am glad you were my teacher. Thank you for your friendship and advice over the years.

Prof. John Field for proofreading my thesis and for sharing the joy you have of writing.

Linda and Dennis Tucker, and **Kirsten and Cathryn Gelderblom**. I will not be where I am today without you. Thank you for always being there for me. I am truly grateful.

And I will not forget **Tanya Marshall** for 'running' alongside me until the 'end of the race'.

Without your help, this study would not have progressed to the position it did. Thank you.

Contents

Declaration iv

Abstract v

Acknowledgements vii

Contents ix

List of Tables xii

List of Figures xiii

Glossary and Acronyms xviii

1 Introduction 1

1.1 Overview of Antarctic Sea Ice 2

1.1.1 Antarctic Marginal Ice Zone *3*

1.2 Observing Antarctic Sea Ice Variability 6

1.2.1 Passive Microwave Observations *6*

1.2.2 Ship-Based Observations *9*

1.3 Aim and Objective 9

2 Data and Methods 11

2.1 *In Situ* SIC Data Collection 11

2.1.1 ASPeCt Protocol Design *11*

2.1.2 Implementation of the ASPeCt Protocol on the S.A. Agulhas II *15*

2.1.3 Ship-Based Sea Ice Protocol Limitations *19*

2.2 Satellite Data PM SIC Retrievals 19

2.2.1 Sea Ice Extent Calculation *20*

2.3 Co-Location and Comparison Method 23

2.4 Automatic Acquisition of Sea Ice Concentration 27

2.4.1 Image Acquisition *27*

2.4.2 Video Pre-Processing *28*

2.4.3 Sea Ice Identification 29

3 RESULTS 31

3.1 Co-Location and Comparison Results 31

3.1.1 Case Study I: Summer 2016 and 2017 31

3.1.2 Case Study II: Winter 2016 and 2017 36

3.1.3 Statistical Analysis 40

3.2 Automatic Acquisition of Sea Ice Concentration 42

3.3 Antarctic Sea Ice Extent: Seasonal and Inter Annual 44

4 DISCUSSION AND CONCLUSIONS 53

4.1 The Assessment Phase 53

4.2 Automatic Acquisition of SIC 57

4.3 Seasonal MIZ SIE Observed through Satellite 60

4.4 Conclusions 63

LIST OF REFERENCES 65

List of Tables

Table 2.1: The ASPeCt Protocol Design for Sea Ice Observations. 13

Table 2.2: The ASPeCt Protocol Design for Meteorological Observations. 14

Table 3.1: Statistical summary of the relationship between the ASI- and BST-AMSR2 SIC estimates and the ship-based SIC observations (OBS). 40

List of Figures

Figure 1.1: Antarctica with the surrounding Southern Ocean. Denoting the climatological September maximum ice extent (purple contour; ~ 18 x 10^6 km^2) and the February minimum ice extent (maroon contour; ~ 3 x 10^6 km^2). The respective shaded areas of ice concentration for September and February are included. 1

Figure 1.2: Schematic of the Antarctic Marginal Ice Zone. Included are illustrations of the metocean processes that contribute to increasing SIC. Where ice concentration is decreasing, these illustrated processes would typically act in the opposite direction. The flow of heat (orange arrows) and warmer water (red arrows) is included. The dark and light blue arrows indicate the flow of water affecting surface freshwater balance and air, respectively (source: Maksym, 2018). 4

Figure 1.3: Images captured at the MIZ edge during the *S.A. Agulhas II* (a) 2017 winter, and (b) 2016 summer expeditions. 5

Figure 1.4: Semi-consolidated ice cover comprised of (a) pancake, (b) frazil, and (c) brash ice. Image taken off the *S.A. Agulhas II* during the 2017 winter expedition. 5

Figure 1.5: (a) Large floe formed from consolidated pancake ice. Characteristic surface roughness features of pancake ice are evident. Image taken off the *S.A. Agulhas II* during the 2016 summer expedition, SANAE 56. 6

Figure 1.6 The red lines show the 1979 – 2017 satellite record. The range of variability is depicted by the blue shaded area (± 1 standard deviation) from a suite of selected global climate models. The inset highlights the satellite monthly ice extent anomalies for 1979 – 2017 (source: Maksym, 2018). 7

Figure 1.7: The trend in annual mean sea ice concentration for 1979 – 2013 (% dec^{-1}). Weddell Sea (W), Indian Ocean (IO), Western Pacific Ocean (WPO), Ross Sea (RS), Amundsen Sea (AS), and Bellingshausen Sea (BS) (source: Turner et al., 2016).....8

Figure 2.1: Flow Chart demonstrating the necessary steps taken which precede the ASPeCt Protocol. 16

Figure 2.2: The SA Aguhass II (Adapted from Soal et al., 2005). 17

Figure 2.3: Images of (a) the TomTom camera used within the Antarctic MIZ and (b) a diagram of the camera set-up. 18

Figure 2.4: Example of a 2D array of retrieved SIC within a given area defined by latitude (rows) and longitude (columns). 21

Figure 2.5: Example of a binary 2D array representing the total SIE retrieved within a given region..... 22

Figure 2.6: Example of a binary 2D array representing the MIZ SIE retrieved within a given region..... 22

Figure 2.7: Polar stereographic ASI-AMSR2 satellite image (3.125 km grid resolution) of SIC (%) covering the Southern Ocean around Antarctica on the days that the *S.A. Agulhas II* first reached the ice edge during (a) each summer expedition on (i) 07 December 2016 and (ii) 18 December 2017, and during (b) each winter expedition on (i) 21 July 2016 and (ii) 04 July 2017. Overlaying the SIC is the ship track (red line) as well as the studied area of ship-based observations (highlighted box).....24

Figure 2.8: A schematic of (a) the co-location method (source: Beitsch et al., 2015). Blue-coloured pixels depict the selected PM grid cells. Pink dots depict the ship points for ship-based SIC observations, and (b) the analysis structure of the co-location method depicted in flow chart form. (Adapted from Beitsch et al., 2015). 25

Figure 2.9: Example of a Taylor Diagram for displaying pattern statistics (source: Taylor, 2001). 26

Figure 2.10: The camera's total FOV providing the (a) view of overturning ice floes, and (b) the edge of the hull. 28

Figure 2.11: The (a) total FOV of the camera, including the highlighted sub-scene, with the (b) extracted grey-scale subscene. Point X marks the brightness reference point.....29

Figure 2.12: Final image showing sea ice (yellow) and water (purple) pixels.....30

Figure 3.1: SIC (%) from the austral summer ship-based observations (colour-coded points) retrieved from (a) 07-10 December 2016, and (b) 18 December 2017. Overlaid on AMSR2 (i) ASI-AMSR2 (3.125 km grid-resolution), and (ii) BST-AMSR2 SIC (12 km grid-resolution) retrievals on (a) 07 December 2016, and (b) 18 December 2017..... 32

Figure 3.2: SIC (%) retrieved from the *S.A. Agulhas II* Antarctic summer (a) 2016, and (b) 2017 expeditions, estimated using ship-based (OBS-SIC; black line), the ASI-AMSR2 (ASI-SIC; blue line), and the BST-AMSR2 (BST-SIC; red line) observations, with respect to Latitude (decimal degrees). The 15% MIZ edge (horizontal, grey, dotted line) is included, along with the latitudinal location of the 15% OBS-, ASI-, and BST-SIC MIZ edge (black, red, and blue vertical lines, respectively).....33

Figure 3.3: First column (i): Ship-based (OBS-SIC; black line), the ASI-AMSR2 (ASI-SIC; blue line), and the BST-AMSR2 (BST-SIC; red line) estimates (%), with respect to Latitude (decimal degrees). SIC retrieved during (a) the first encounter of sea ice, and (b) after exiting the polynya. The 15% MIZ edge (grey, dotted line) is included, along with the latitudinal location of the 15% OBS-, ASI- and BST-SIC MIZ edge (black, red and blue vertical lines, respectively). Second column (ii): images taken off the *S.A. Agulhas II* at the MIZ edge.....35

Figure 3.4: First column (i): Ship-based (OBS-SIC; black line), the ASI-AMSR2 (ASI-SIC; blue line), and the BST-AMSR2 (BST-SIC; red line) estimates (%), with respect to Latitude (decimal degrees). SIC retrieved during (c) the *S.A. Agulhas II* exiting the MIZ edge. The 15% MIZ edge (grey, dotted line) is included, along with the latitudinal location of the 15% OBS-, ASI- and BST-SIC MIZ edge (black, red and blue vertical lines, respectively). Second column (ii): image taken off the *S.A. Agulhas II* of the MIZ edge.....36

Figure 3.5: SIC (%) from the austral winter ship-based observations (colour-coded points) retrieved from (a) 21 – 22 July 2016, and (b) 04 – 05 July 2017. Overlaid on AMSR2 (i) ASI-AMSR2 (3.125 km grid-resolution), and (ii) BST-AMSR2 SIC (12 km grid-resolution) retrievals on (a) 21 July 2016, and (b) 04 July 2017. The red and orange lines represent the ship entering and exiting the sea ice environment, respectively. 37

Figure 3.6: First column (i): SIC (%) retrieved from the *S.A. Agulhas II* Antarctic winter (a) 2016, and (b) 2017 expeditions; estimated using ship-based (OBS-SIC; black line), the ASI-AMSR2 (ASI-SIC; blue line), and BST-AMSR2 (BST-SIC; red line) observations, with respect to Latitude (decimal degrees). The 15% MIZ edge (horizontal, grey, dotted line) is included, along with the latitudinal location of the 15% ASI- and BST-SIC MIZ edge (red and blue vertical lines, respectively). Second column (ii): image taken off the *S.A. Agulhas II* of the respective winter MIZ edges..... 38

Figure 3.7: Images showing the high MIZ SIC (%) captured aboard the *S.A. Agulhas II* during the winter (a) 2016 (90% SIC), and (b) 2017 (100% SIC) expeditions. 39

Figure 3.8: Taylor Diagrams showing the relationship between the ship-based SIC observations with the ASI-AMSR2 and BST-AMSR2 SIC estimates for the (i) summer 2016, (ii) summer 2017, and (iii) winter 2017 South African Antarctic expeditions. 41

Figure 3.9: SIC (%) retrieved along latitude (decimal degrees) from ship-based (OBS-SIC; black line), and the algorithm designed to automatically acquired SIC (purple line) for (a) the summer 2016 and (b) the winter 2017 expeditions aboard the *S.A. Agulhas II*. 43

Figure 3.10: Daily Antarctic sea ice extents for the climatology (1981 – 2010; red line), 2016 (dotted black line) and 2017 (solid black line). 45

Figure 3.11: Anomalies indicative of the (a) inter annual, and (b) seasonal variation in sea ice extent from the climatology over the past twenty-one years (1997 - 2017). Values are derived from the satellite passive microwave data from Special Sensor Microwave/Sounder using the ARTIST sea ice algorithm. 46

Figure 3.12: Monthly Atlantic Ocean ice extents for the climatology, 2015, 2016, 2017, and averaged over 3-year periods 1997 - 1999 through 2012 - 2014. Values are derived from ASI-SSMIS. 47

Figure 3.13: (a) The Antarctic MIZ edge from ASI-SSMIS for 2016 (gold contour), and 2017 (red contour), and the SIC for the climatology (colour-coded), when the ice cover reached its annual maximum extent in September. The Weddell, Lazarev and Riiser-Larsen sectors are highlighted in purple, green and orange, respectively. Included are (b) the September sea ice anomalies from 2016 and 2017. 48

Figure 3.14: The (i) blue and red line present the total SIE (0% - 100% SIC) and the MIZ SIE (15% - 80% SIC), respectively. The (ii) ratio (MIZ SIE/Total SIE) is included. These results are specific to the (a) Weddell, (b) Lazarev, and (c) Riiser-Larsen sectors. 50

Figure 4.1: Sub-scene image stills depicted in (a) grey scale and (b) binary after using the threshold method: yellow and purple are ice and water, respectively. In the interstices of the pancakes are (i) brash and (ii) frazil ice. A few surface melt signatures in the centre of the pancakes are denoted in red. 59

Figure 4.2: Orthorectified image of the subscenes presented in Figure 4.1..... 60

Glossary and Acronyms

AMSR2	Advanced Microwave Scanning Radiometer 2
ARTIST	Arctic Radiation and Turbulence Interaction STudy
ASI	ARTIST Sea Ice
Austral Autumn	March, April, May
Austral Spring	September, October, November
Austral Summer	December, January, February
Austral Winter	June, July, August
BST	Bootstrap
ASPeCt	Antarctic Sea Ice Processes and Climate
MIZ	Marginal Ice Zone
PM	Passive Microwave
RMSD	Root-Mean-Square Difference
S.A.	South African
SANAE	South African National Antarctic Expedition
SCAR	Scientific Committee on Antarctic Research
SIC	Sea Ice Concentration
SIE	Sea Ice Extent
SSMIS	Special Sensor Microwave/ Imager Sounder
T_b	brightness temperature

I Introduction

The Antarctic continent is surrounded by seasonally varying sea ice that advances northward in the austral autumn and winter and retreats in the spring and summer. At maximum annual ice extent, the sea ice can extend as far as 2500 km from the Antarctic continent (Petrich and Eicken, 2010; de Jong, 2016) covering approximately 18 x 10^6 km^2 of the Southern Ocean, whereas only 3 x 10^6 km^2 is covered during summer (Figure 1.1; Davies, 2015; de Jong, 2016). This seasonal sea ice variability is the annual pattern from which climate change trends are quantified using satellite remote sensing observations. Through these observations, sea ice concentration (SIC, a measure of the proportion, recorded as a percentage, of ice-covered water to water not covered by ice) is obtained and sea ice extent (SIE) can be calculated. SIE is a measure of the surface area of the ocean where sea ice is observed from its northern-most latitudinal location. This may include areas of no or very low SIC present (i.e. polynyas).

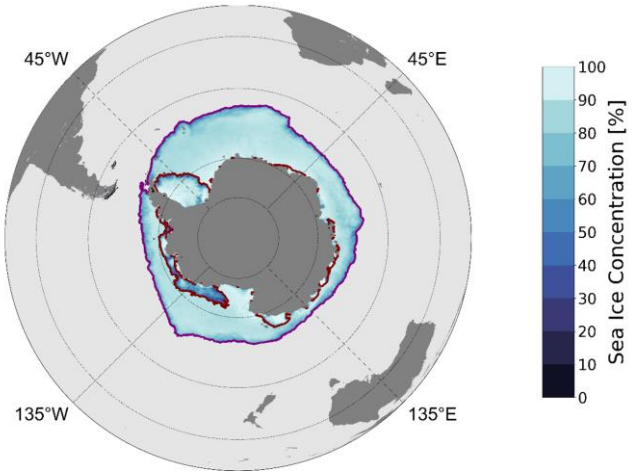

Figure 1.1: Antarctica with the surrounding Southern Ocean. Denoting the climatological September maximum ice extent (purple contour; ~ 18 x 10^6 km^2) and the February minimum ice extent (maroon contour; ~ 3 x 10^6 km^2). The respective shaded areas of ice concentration for September and February are included.

A notable difference between the Antarctic and Arctic regions is the fact that Antarctic sea ice is unbounded by land (Figure 1.1). A consequence of this is that the interactions between the atmosphere, ice, and ocean in the Southern Ocean are markedly different in comparison to those of the Arctic (Maksym, 2018). For example, the Antarctic sea ice-cover is exposed to warmer maritime air masses relative to the Arctic, resulting in more complex sea ice surface physical conditions (Cavalieri et al., 2010). The extent of SIC is typically monitored using satellite-based passive microwave (PM) remote sensing techniques. However, most algorithms employed to achieve these SIC observations were mostly tested for the Arctic environment (Cavalieri et al., 2010) and, therefore, when applied to the Antarctic, do not adequately account or the unbounded nature of the sea ice in the Southern Ocean. These PM SIC measurements, designed for Arctic observations, set a threshold minimum at 15% SIC and, therefore, correspond most closely with the average true marginal ice zone (MIZ) edge (Comiso, 2006; Meier and Stroeve, 2008). The MIZ is an area of ice cover which is close enough to the open ocean boundary to be affected by the proximity of the open ocean (Wadhams, 1986). Furthermore, this 15% minimum SIC threshold eliminates unrealistic values caused by the influence of wind and weather in the near-open ocean region (Worby and Comiso, 2004). As a result, SIC lower than 15% is difficult to derive through PM-estimates, which poses a concern because, if high resolution PM SIC observations are to be used for any Antarctic research field, then the accuracy of the estimated SIC needs to be known. In the event that Antarctic MIZ SIC recoveries are not well understood, ship track planning and navigation may be erroneous, or studying seasonal and inter annual sea ice patterns may be misinterpreted.

1.1 Overview of Antarctic Sea Ice

In 1991, a meeting was hosted by the Scientific Committee on Antarctic Research (SCAR), *The Role of Antarctica in Global Change*. During this meeting, the Southern Ocean sea ice region (the area which acts as a regional boundary between sub-Antarctica and the Antarctic continent) was identified as one of the most important areas where global change will be manifest (ASPeCt, 1998-2008; de Jong, 2016). The important role

sea ice plays in the climate system is a result of certain characteristics that sea ice possesses. These include, high albedo relative to the underlying ocean, the effect sea ice has on the near-surface freshwater flux, and its impact on heat and moisture transport between the atmosphere and ocean (Meier and Stroeve, 2008). These sea ice characteristics contribute as an indicator of climate change, therefore, understanding its variability is required for projecting future climate variability and change (Matear et al., 2015). For example, intense ice-ocean-atmosphere interactions take place within the MIZ, therefore, an expanding or retreating MIZ may help to shed light on the metocean processes (i.e. the combination of meteorological and oceanographic variables) impacting the observed trends in sea ice variability within the Southern Ocean (Stroeve et al., 2016). However, relatively little attention has been given to the processes by which the Antarctic MIZ forms and responds to synoptic events.

1.1.1 Antarctic Marginal Ice Zone

The MIZ forms a part of the Antarctic sea ice environment and is specifically referred to as the boundary between continuous ice-covered seas and the open ocean (Figure 1.2, Collins et al., 2015). Passive microwave satellites typically define the MIZ to be between 15% (corresponding to the conventional MIZ edge (Comiso, 2006; Meier and Stroeve, 2008)) and 80% SIC (defined by the World Meteorological Organization as 'close ice' (WMO, 2009)). The seasonal maximum northward Antarctic sea ice edge is limited primarily by the Antarctic Circumpolar Current (Martinson, 2012) and is buffeted by the impact of the strongest winds and waves on Earth (Maksym, 2018). Sea ice forms within the MIZ and, therefore, these ocean and atmosphere interactions influence the formation, consolidation and subsequent melt of the MIZ (Weeks and Ackley, 1982), thus inducing the formation of its heterogeneous semi-solid matrix. On a geophysical scale, relative to the ocean and atmosphere bodies, sea ice is merely a thin, fragile blanket covering the ocean surface (Figure 1.2; Weeks and Ackley, 1986; Dieckman and Hellmer, 2010).

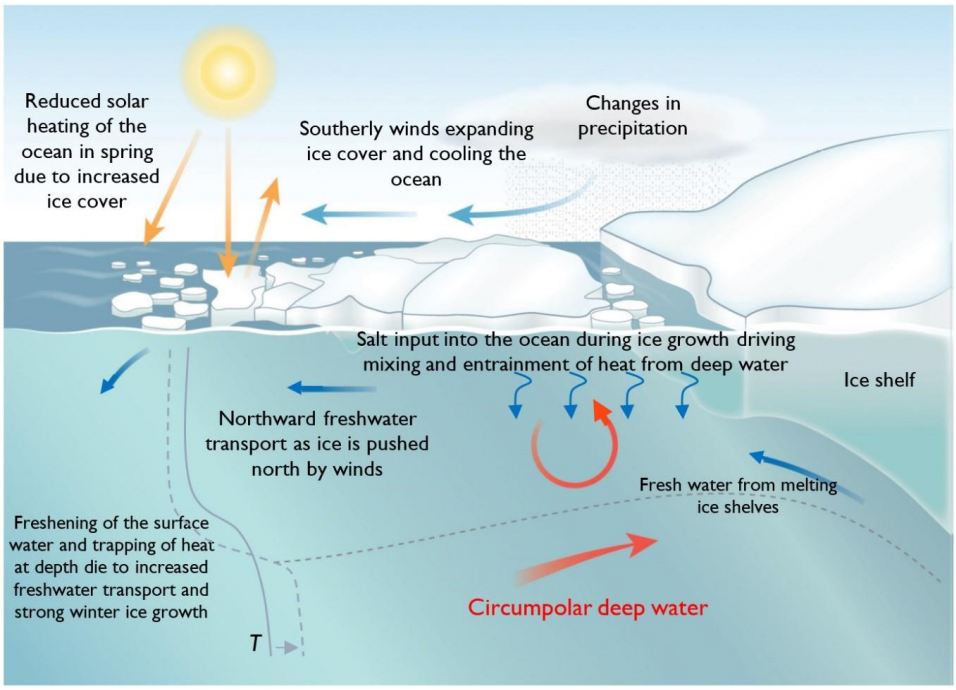

Figure 1.2: Schematic of the Antarctic Marginal Ice Zone. Included are illustrations of the metocean processes that contribute to increasing SIC. Where ice concentration is decreasing, these illustrated processes would typically act in the opposite direction. The flow of heat (orange arrows) and warmer water (red arrows) is included. The dark and light blue arrows indicate the flow of water affecting surface freshwater balance and air, respectively (source: Maksym, 2018).

The growth of the Antarctic MIZ is triggered by southerly winds which cool the ocean surface (Figure 1.2), and is dominated by frazil (small, needle-like ice crystals) and pancake (a highly viscous fluid, lying on top of an inviscid ocean (Wadhams et al., 2004)) ice (Doble and Wadhams, 2006). Growth of individual frazil crystals in a supercooled water column should be seen in context with the growth of congelation ice (thick and more stable ice sheet) insofar as both heat and salt need to be transported away from the interface into the surrounding ocean water. Subsequently, when the frazil platelets are beyond a certain size, they further develop tough, dendritic surfaces due to solute build-up (Petrich and Eicken, 2010; de Jong, 2016).

Turbulent oceanic conditions can break up the ice hundreds of kilometres inside the MIZ edge (Kohout et al., 2014). This causes the MIZ to comprise of scattered and relatively small and thin pieces of ice floes (Beitch et al., 2015). In winter, a combination of frazil growth and brash (fragmented floating ice) ice are commonly located in the

interstices between the individual pancakes (Figures 1.3a and 1.4), whereas in summer, brash and melting ice are predominant (Figures 1.3b and 1.5).

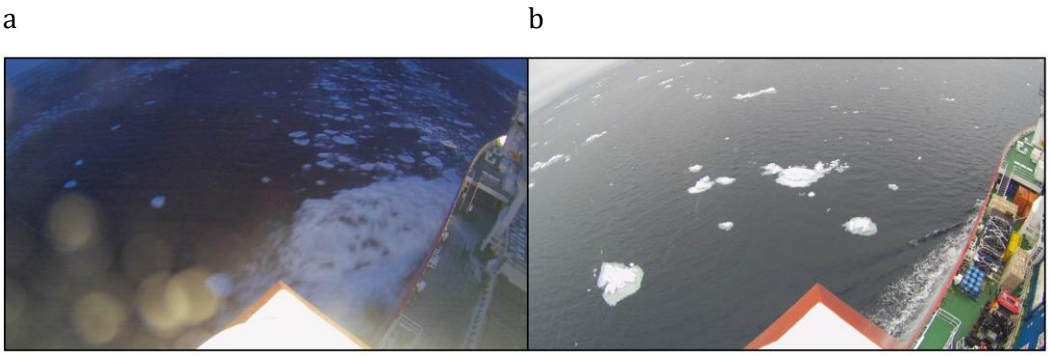

Figure 1.3: Images captured at the MIZ edge during the *S.A. Agulhas II* (a) 2017 winter, and (b) 2016 summer expeditions.

During winter, pancake ice development within the MIZ is predominant as a result of this dynamic environment favouring the initial growth of frazil ice: through the accretion of frazil platelets, the ice forms into centimetre-sized floes that, in turn, accrete into decimetre-sized pans of ice, namely pancake ice. These pancakes develop from a few centimetres to more than 10 cm thick and, over time, congeal into larger units (Figure 1.4; de Jong, 2016).

Figure 1.4: Semi-consolidated ice cover comprised of (a) pancake, (b) frazil, and (c) brash ice. Image taken off the *S.A. Agulhas II* during the 2017 winter expedition.

The conversion of the ice cover from pancake to pack ice is influenced by waves propagating from the open Southern Ocean into the MIZ (Doble et al., 2015). Once the

ice cover has consolidated into a solid, continuous sheet of large pancakes with accumulated snow on the surface, only characteristic surface roughness features betray its dynamic origins (Figure 1.5; Petrich and Eicken, 2010; de Jong, 2016).

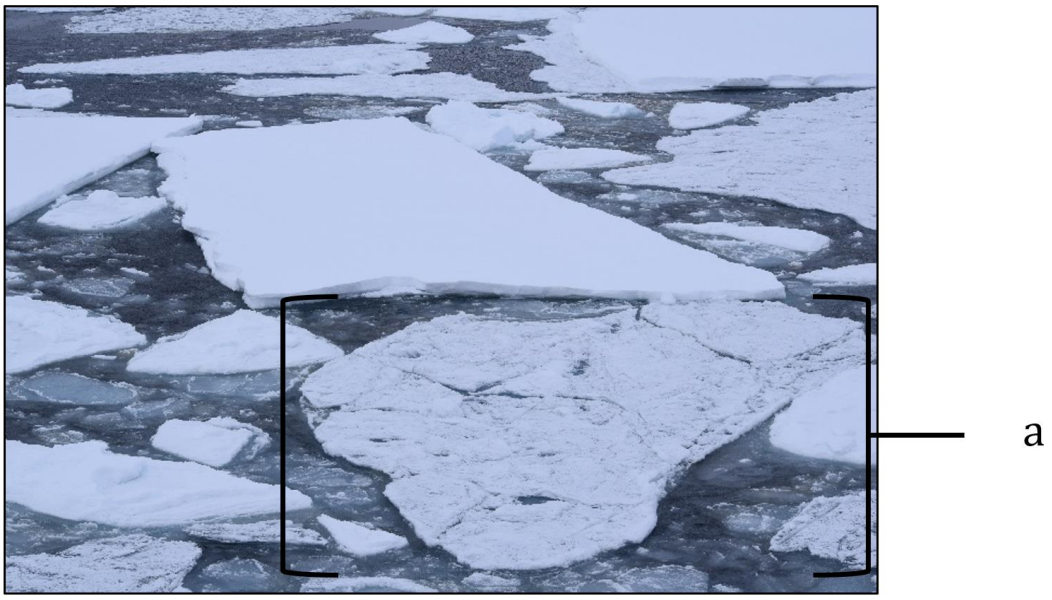

Figure 1.5: (a) Large floe formed from consolidated pancake ice. Characteristic surface roughness features of pancake ice are evident. Image taken off the *S.A. Agulhas II* during the 2016 summer expedition, SANAE 56.

Overall, sea ice cover varies throughout the year in both extent and type. A common way of achieving insight into this seasonal variability is through both satellite and *in situ* observations.

1.2 Observing Antarctic Sea Ice Variability

Antarctic sea ice variability strongly depends on the time period and season (Section 1.1; Maksym, 2018). This section will focus on two main techniques used to observe Antarctic seasonal and inter annual variability.

1.2.1 Passive Microwave Observations

The broad spatial coverage and the high spatial and temporal variability of sea ice is effectively monitored via PM satellite remote-sensing instruments, covering all-sea-ice areas and monitoring ice in all-sky conditions (Meier and Stroeve, 2008). The record of

reliable PM satellite SIE estimates began in late-1978 (Turner et al., 2016). As a result, the satellite era has enabled a host of breakthroughs over the past 30 years; leading to remote sensing of sea ice as a back-bone for polar sea ice research and understanding.

Over the past few years, sea ice variability has increased in both hemispheres. In the Antarctic, however, the recent variability has been relatively more dramatic (Maksym, 2018). Three consecutive years of record high SIE occurred from 2012 – 2014, followed by record low SIE anomalies recorded in spring 2016 and 2017 (Figure 1.6). This is seen by the red line highlighted by the inset in Figure 1.6. These record-low anomalies rivalled those documented in the Arctic summer and, as reported by Maksym (2018), were large enough to erase the statistical significance of the previously reported increasing Antarctic SIE trends (excluding recordings in autumn). Such results emphasize the need for additional investigations to confirm previous trends.

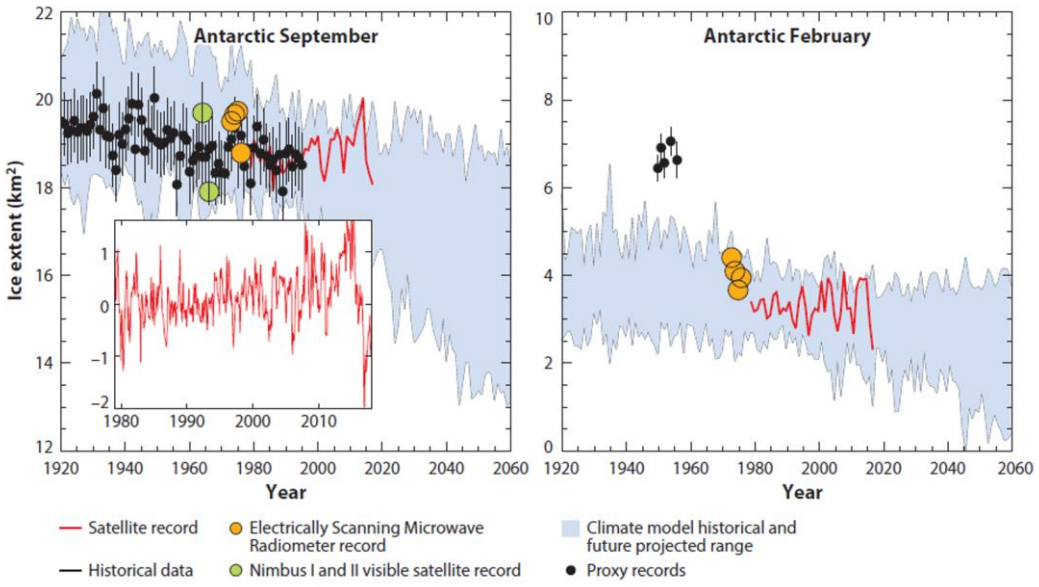

Figure 1.6 The red lines show the 1979 – 2017 satellite record. The range of variability is depicted by the blue shaded area (± 1 standard deviation) from a suite of selected global climate models. The inset highlights the satellite monthly ice extent anomalies for 1979 – 2017 (source: Maksym, 2018).

The overall Antarctic SIE increasing (from 1978 – 2014) and decreasing (through 2016 – 2017) trends has, however, masked large regional variations. Therefore, it is important to observe sea ice variability on a regional scale (e.g. Comiso et al., 2011; Stammerjohn et al., 2012; Turner et al., 2016). For example, although there was an average

increase in SIE from 1979 – 2013 (Figure 1.6), Figure 1.7 shows an average decrease in SIE within the Bellingshausen Sea.

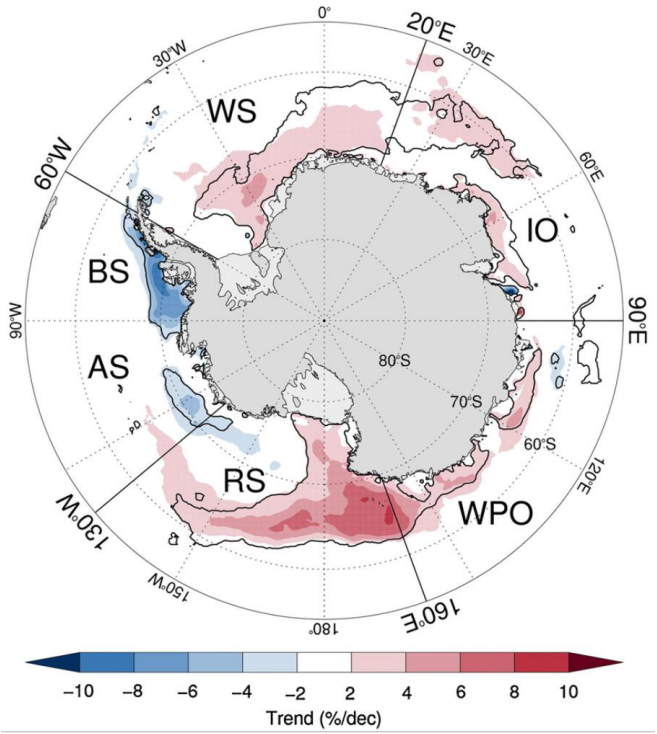

Figure 1.7: The trend in annual mean sea ice concentration for 1979 – 2013 (% dec^{-1}). Weddell Sea (W), Indian Ocean (IO), Western Pacific Ocean (WPO), Ross Sea (RS), Amundsen Sea (AS), and Bellingshausen Sea (BS) (source: Turner et al., 2016).

Considering regional heterogeneity is important for in-depth understanding of seasonal and inter annual SIE trends. In general, processes contributing towards regional heterogeneity, such as ice-ocean and ice-atmosphere interactions and feedbacks, are poorly observed. Stroeve et al. (2016) shows that, to better understand regional as well as total changes in Antarctic sea ice, changes in the MIZ need to be included. Should our understanding of the total and MIZ sea ice environment improve (on a global as well as a regional scale), then a sustained network of both satellite and *in situ* observations is required.

1.2.2 Ship-Based Observations

Although *in situ* SIC observations are limited because of spatial and temporal restrictions, unique features and characteristics of sea ice regions can still be provided. Such information can be collected through ship-based observations using the Antarctic Sea Ice Processes and Climate (ASPeCt) protocol which is standardised, quantifiable, and accepted as the international standard for sea ice characteristic and thickness observations (Worby and Allison, 1999; ASPeCt, 2018). This multi-disciplinary Antarctic sea ice research programme has an overall aim to understand and model the role of Antarctic sea ice, while their key objective is to improve regional understanding, accomplished through ongoing field programmes, remote sensing and numerical modelling. Comparative analysis methods have been developed from several studies that have used voyages contributing to ASPeCt data as a ground truth data source for evaluating satellite PM SIC products (e.g. Spreen et al., 2008; Heygster et al., 2009; Beitsch et al., 2015; Pang et al., 2018).

1.3 Aim and Objective

The objective of this study is to compare sea ice observations from the *S.A. Agulhas II* to high resolution PM satellite imagery, focussing on the heterogeneous MIZ in the years of 2016 and 2017. Ice concentration was investigated to evaluate the quality of satellite retrievals with respect to ship-based observational estimates, based on the ASPeCt protocol. To maximize the retrieval of information from previous cruises not specifically dedicated to sea ice observations, an algorithm was developed to automatically retrieve SIC from pre-existing images and videos. This method, based on the use of off-the-shelf action cameras, can be used to obtain quantitative sea ice data from vessels of opportunity without the need to have trained personnel on-board. This study aims to assess the seasonal SIE of the MIZ by comparing sea ice observations estimated from aboard ship to high resolution PM satellite imagery when transecting the MIZ. This comparison will allow an understanding of the shortcomings inherent in SIC derived

from PM satellite products. The study addresses the following longer-term scientific question:

> What is the seasonal MIZ sea ice extent estimated by passive microwave within the Atlantic sector?

The primary focus of the study is on the spatial sea ice characteristics of the unique Antarctic MIZ environment. More specifically, the Atlantic sector was the focus using recent anomalous years (2016 – 2017) because there were more *S.A. Agulhas II* observations available within this region and time period. Remote sensing is one way to obtain high resolution images of sea ice surface features, however these need to be assessed in combination with direct observations. Therefore, the previously stated aim was achieved by

i. Combining complementary observations from the *S.A. Agulhas II* and satellite passive microwave records to assess the quality of remote sensing data in the Atlantic MIZ,
ii. Exploring an algorithm to automatically acquire SIC from image stills and videos, and,
iii. Determining the seasonal MIZ sea ice extent by passive microwave.

2 Data and Methods

This chapter provides a detailed description of SIC retrieval methods used throughout this study, namely, ship-based observations, and high-resolution PM satellite estimates.

2.1 *In Situ* SIC Data Collection

This section first provides a thorough explanation of ship-based sea ice observations, using the ASPeCt protocol, and how these observations were conducted during the *S.A. Agulhas II* 2016 and 2017 summer and winter expeditions. These ASPeCt observations have been implemented aboard the *S.A. Agulhas II* since the 2016 winter expedition where SCAR sponsored the training with a professional Arctic observer.

2.1.1 ASPeCt Protocol Design

The way in which the ASPeCt protocol sets up the methodological design for ship-based observations of the sea ice environment is of importance. It provides all key elements within the sea ice environment, including ocean-ice-atmosphere variables, which enhances the external reader's understanding of what the on-board observers experienced while conducting observations. These trained observers learned the standard ASPeCt protocol (introduced in Section 1.2.2) as well as sea ice observation procedures. Tables 2.1 and 2.2 summarizes the sea ice and meteorological observation design of the ASPeCt protocol, respectively.

Table 2.1: The ASPeCt Protocol Design for Sea Ice Observations.

Day/Date (Z):								
	POSITION			SEA ICE OBSERVATIONS				
hr (Z)	Lat (°S) dd mm	Lon (°E/W) ddd mm	Conc (tenths)	PRIMARY c ty z f t s sz	SECONDARY c ty z f t s sz	TERTIARY c ty z f t s sz	O/W	hr (Z)
0								0
1								1
2								2
3								3
4								4
5								5
6								6
7								7
8								8
…								…
23								23
NOTES: *PRIMARY SEA ICE IS OF GREATEST THICKNESS. HENCE z1 > z2 > z3								

Table 2.2: The ASPeCt Protocol Design for Meteorological Observations.

Day/Date (Z):												
	METEOROLOGICAL OBSERVATIONS						PHOTO	VIDEO	COMMENTS		OBSERVER	
hr (Z)	Twater (°C)	Tair (°C)	Wind (sp/d)	Cloud (oktas)	Visb (v)	Weath (ww)	Film/Frame	Tape No/ Reading	Text	Ref. no	Name	hr (Z)
0												0
1												1
2												2
3												3
4												4
5												5
6												6
7												7
8												8
…												…
23												23
NOTES: *ADDITIONAL COMMENTS CAN BE PROVIDED ON A SEPARATE COMMENTS PAGE, PROVIDED DUE REFERENCE IS GIVEN												

The sea ice environment consists of three main sea ice states; the Primary, Secondary, and Tertiary states. The Primary state is the thickest sea ice observed in the environment and is usually the dominant ice type present. Thinner than the Primary state are the Secondary and Tertiary states; with the Secondary being thicker than the Tertiary. The sea ice environmental conditions are observed hourly (as detailed in Tables 2.1 and 2.2) and begin the instant the ship enters the ice environment and stops when the ship has either reached its destination or exited the ice.

During each Antarctic *S.A. Agulhas II* expedition, a team of ship-based observers recorded the surrounding sea ice environment hourly (hr), including the ship's latitudinal (Lat (°S)) and longitudinal (Long (°E/W)) location with total SIC (Conc (tenths)) recorded in percentage values of tenths. Furthermore, the ice environment characteristics for each of the three sea ice states was recorded. This included an estimation of the areal coverage in concentration (c), ice type (ty), as well as thickness (z), floe size (f), topography (t), and type of snow cover (s) with snow thickness (sz) (Table 2.1). Observations were conducted within an approximate 1 km radius around the ship. The limitations associated with the ship-based observers recording the sea ice environment, specific to *S.A. Agulhas II* expeditions, are detailed in Section 2.1.3.

The meteorological observations for each hourly recording included water and air temperature (T_{water} and T_{air} (°C), respectively), wind speed, cloud cover (recorded in oktas), visibility, and weather (Table 2.2). These observations were conducted over a 360-degree view and depended on visibility.

2.1.2 Implementation of the ASPeCt Protocol on the *S.A. Agulhas II*

First and foremost, the procedure detailed in Figure 2.1 was followed before the initiation of the ASPeCt protocol procedure. This initial step is important because the ASPeCt protocol does not include camera-setup. This section, therefore, details the design to combine ASPeCt observations with automatically acquiring SIC from image stills and videos which, additionally, provides a platform for post-expedition SIC-retrieval validation if the ship-based observers are known to be inexperienced.

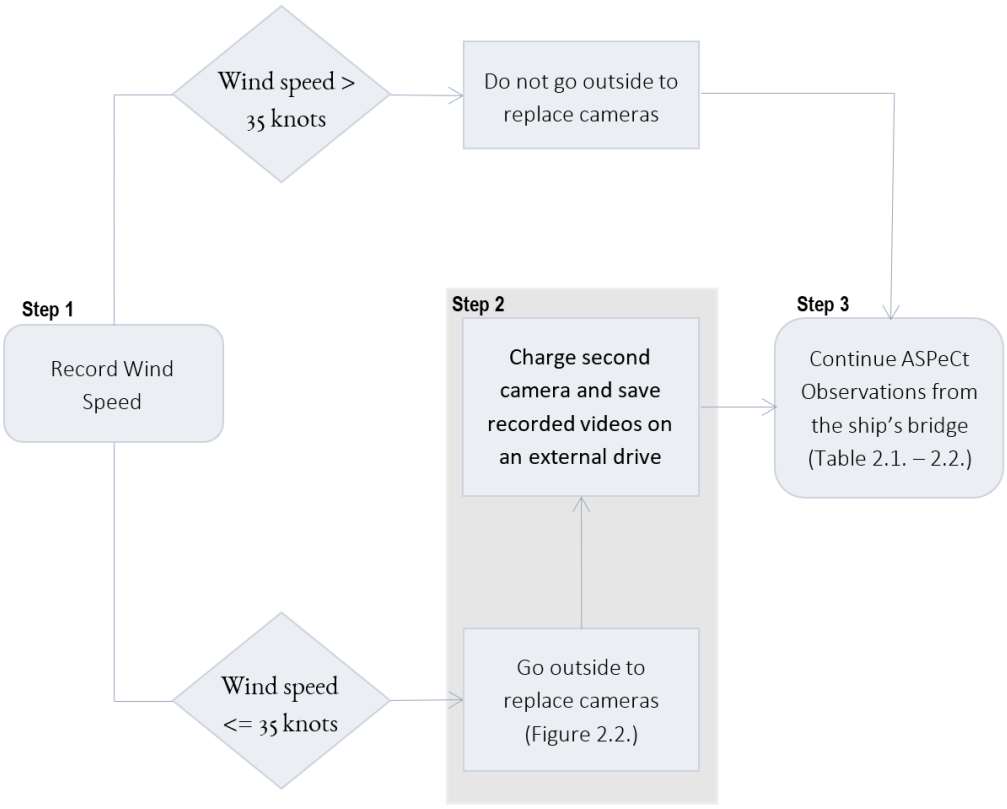

Figure 2.1: Flow Chart demonstrating the necessary steps taken which precede the ASPeCt Protocol.

Previous winter voyages off the *S.A. Agulhas II* experienced wind speeds of 45 knots, swells reaching 7 m, and wind chills reaching -20 °C. These harsh Antarctic environmental conditions are considered dangerous to work in.

The ship-based observation procedure was broken down into three main steps for every hourly observation. Firstly, the on-board observer on duty will retrieve wind speed readings from the bridge (see Figure 2.2). If the wind speed is greater than 35 knots the observer will remain on the bridge and continue directly to step three (see Section 2.1.1). However, if the wind speed is less than or equal to 35 knots, the observer will continue to step two (detailed in this section) and then to step three. To understand where each step takes place, a diagram of the *S.A. Agulhas II* is shown overleaf:

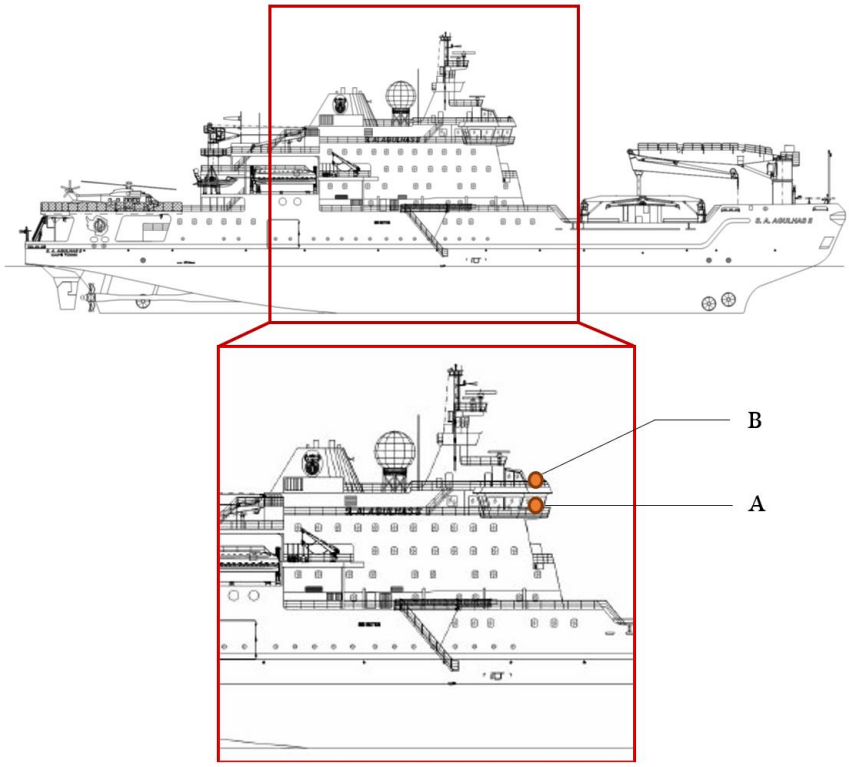

Figure 2.2: The *S.A. Agulhas II* (Adapted from Soal et al., 2005).

The exterior design of the *S.A. Agulhas II* is shown in Figure 2.2. Position A is the ship's bridge, where the ASPeCt observations take place (step three as described in Section 2.1.1). Position B is the 'Monkey Island' - located directly above the bridge - where the camera set up and recordings take place (step two as described in this section).

Focussing on step two, for ship-based observation recordings, an off-the-shelf TomTom video camera is mounted on a clamp on the 'Monkey Island' (Position B), as depicted in Figure 2.3. TomTom video cameras were used as they provide GPS readings, have weather-proof casing against snow and rain, and are designed to be taken on and off the stand and charged efficiently. Two cameras are used to achieve continuous replacement (see step 2 in Figure 2.1).

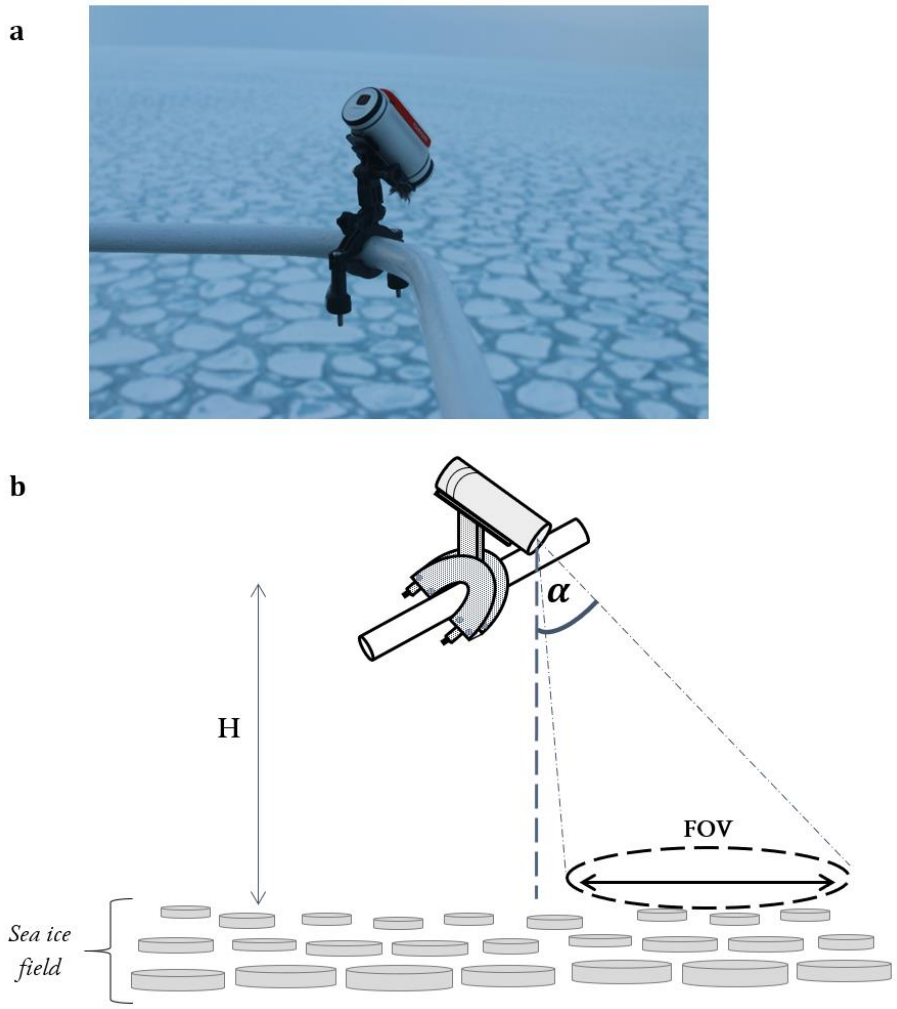

Figure 2.3: Images of (a) the TomTom camera used within the Antarctic MIZ and (b) a diagram of the camera set-up.

This TomTom camera is mounted on a bar 25.22 m (H) above sea level and is set at an angle, α, of 64.5 degrees. This exact angle is not important for every expedition. It is, however, important that once the camera is set up, the angle remains the same throughout the expedition (see Figure 2.3). After mounting, a 1 s time-lapse video is recorded for two hours. At the end of each recording, the observer on duty replaces the camera with a second camera. The wide angled images retrieved from the time-lapse videos provide a field of view (FOV) of approximately 53 m x 76 m for a defined time in space.

Step two detailed above followed with charging the video camera taken off the mount and the data was immediately downloaded onto an external drive. This took place in the bridge and was followed by step three, detailed in Section 2.1.1.

2.1.3 Ship-Based Sea Ice Protocol Limitations

During the *S.A. Agulhas II* Antarctic expeditions, 6 on-board sea ice observers followed a 3-step process detailed from Section 2.1.1 – 2.1.2. However, there were uncertainties linked to the ship-based data collected. Beitsch et al. (2015) and Wagner and Pena (2016) suggested that *in situ* results are subjective and prone to contain errors that vary between observers due to the inevitability of each observer's individual bias. An observer's individual perception of the sea ice conditions may cause inconsistencies in the observer's results (de Jong, 2016; Wagner and Pena, 2016). de Jong (2016) recorded SIC observation differences between 7 observers who lacked experience within the sea ice field. These results found that when inexperienced observers record SIC, the estimates could differ from each observer by approximately 20% SIC. To account for these subjective biases, a method to automatically acquire SIC was developed (Section 2.4).

2.2 Satellite Data PM SIC Retrievals

In addition to SIC retrievals collected aboard ships, a second retrieval method commonly used for Polar research is that of high-resolution PM satellite data (as introduced in Section 1.2.1). For this study, we wanted to use data available at the highest resolution, and therefore used the PM AMSR2 sensor. However, due to uncertainties inherent in different algorithms, two AMSR2 products were used. These were the ARTIST (Arctic Radiation and Turbulence Interaction STudy) sea ice and the bootstrap advanced microwave scanning radiometer 2 (ASI- AMSR2, and BST- AMSR2, respectively).

The AMSR2 satellite product has been retrieving sea ice data since August 2012 using brightness temperatures (T_b), which is the temperature a blackbody would be to emit the same amount of radiation as the observed sea ice floe. The ASI- and BST-

AMSR2 products use sea ice information from higher (89 GHz) and lower (37 GHz) frequencies, respectively. This results in an increased spatial resolution for the ASI-AMSR2 (3.125 km grid resolution; refer to Kaleschke et al. (2001b) and Spreen et al. (2008) for details), and a lower spatial resolution (12.5 km) for the BST- AMSR2 product (detailed in depth by Comiso (1995)). For this study, the ASI- AMSR2 SIC dataset was downloaded from ftp://ftp-projects.cen.uni-hamburg.de/seaice/AMSR2/, and BST-AMSR2 from https://seaice.uni-bremen.de/start/data-archive/.

2.2.1 Sea Ice Extent Calculation

In addition to using the ASI- and BST- AMSR2 satellite products to analyse the Antarctic MIZ, the ASI-SSMIS (Special Sensor Microwave/ Imager Sounder), with a grid resolution of 12.5 km, was used to evaluate the seasonal and inter annual SIE patterns. This datum was retrieved from ftp://ftp.ifremer.fr/ifremer/cersat/products/gridded/psi-concentration/data/antarctic/. For a detailed description of this product, refer to Kaleschke et al. (2001a). The ASI-SSMIS product provides consistent SIC data over an extended time period (from 05.12.1991 – present) and was used in this study when working with long-term data to study the seasonal and inter annual Antarctic variability. To analyse this variability, SIE was calculated from SIC which was retrieved from ASI-SSMIS data. An example of the retrieved SIC data is presented in the 2D array, Figure 2.4.

0	0	0	0	0	0	0	0	0
0	0	0	0	0	0	0	0	0
0	0	0.08	0.11	0.15	0.14	0.11	0.05	0
0	0.12	0.14	0.28	0.16	0.20	0.38	0.17	0
0	0.28	0.15	0.31	0.39	0.40	0.59	0.24	0.15
0.21	0.30	0.32	0.59	0.58	0.41	0.62	0.40	0.25
0.47	0.31	0.62	0.73	0.65	0.84	0.88	0.77	0.74
0.39	0.44	0.81	0.82	0.82	0.98	0.94	0.87	0.96

Figure 2.4: Example of a 2D array of retrieved SIC within a given area defined by latitude (rows) and longitude (columns).

The columns and rows in Figure 2.4 represent a geographic region defined by longitudes and latitudes, respectively. Each box depicts a grid cell which provides a SIC value retrieved on a given day. These SIC values are presented as decimals (i.e. 8% SIC is 0.08).

Due to the aim defined for this study (Section 1.3), it was important to calculate both the total and the MIZ SIE. The total SIE was calculated by extracting each grid cell with a SIC value greater than or equal to 0.15 (because the MIZ edge is defined at 15% SIC (as cited by Meier and Stroeve (2008) in Chapter 1)) and set to 1; as depicted in Figure 2.5.

0	0	0	0	0	0	0	0	0
0	0	0	0	0	0	0	0	0
0	0	0	0	1	0	0	0	0
0	0	0	1	1	1	1	1	0
0	1	1	1	1	1	1	1	1
1	1	1	1	1	1	1	1	1
1	1	1	1	1	1	1	1	1
1	1	1	1	1	1	1	1	1

Figure 2.5: Example of a binary 2D array representing the total SIE retrieved within a given region.

However, to specifically calculate the MIZ SIE, grid cells are set to 1 when a SIC value is greater than or equal to 0.15 (15%) and less than or equal to 0.80 (80%) (The MIZ is operationally defined between 15% - 80% SIC (as defined in Chapter 1)). Figure 2.6 provides an example of building a binary 2D array from extracting MIZ SIC from Figure 2.4.

0	0	0	0	0	0	0	0	0
0	0	0	0	0	0	0	0	0
0	0	0	0	1	0	0	0	0
0	0	0	1	1	1	1	1	0
0	1	1	1	1	1	1	1	1
1	1	1	1	1	1	1	1	1
1	1	1	1	1	0	0	1	1
1	1	0	0	0	0	0	0	0

Figure 2.6: Example of a binary 2D array representing the MIZ SIE retrieved within a given region.

After building a binary 2D array with respect to latitude and longitude, the grid cells set to 1 were multiplied by the grid cell area (12.5 km x 12.5 km for ASI-SSMIS) and

summed. Finally, the monthly mean SIE was calculated over the past 21 years (1996 – 2017). This process was automated using the Python programming language which is ideal for developing complex scientific and numeric applications.

2.3 Co-Location and Comparison Method

The 2016 and 2017 expeditions, aboard the *S.A. Agulhas II*, started in Cape Town, South Africa (34˚54' S, 18˚ 25' E). In summer, these expeditions continued southwest until 0˚ Longitude (the Good Hope Line). Continuing southward along the Good Hope Line, the ship sailed through the sea ice until reaching the Antarctic continent at 69˚ 17' S (Figure 2.7a). During the 2016 and 2017 winter expeditions, the ship navigated toward the Good Hope Line and 30° E, respectively, and, from there, travelled southward until reaching the Antarctic MIZ (Figure 2.7b). Figure 2.7 provides a summary of the ship tracks (red line) and the region in which sea ice observations were conducted (highlighted box) for each expedition.

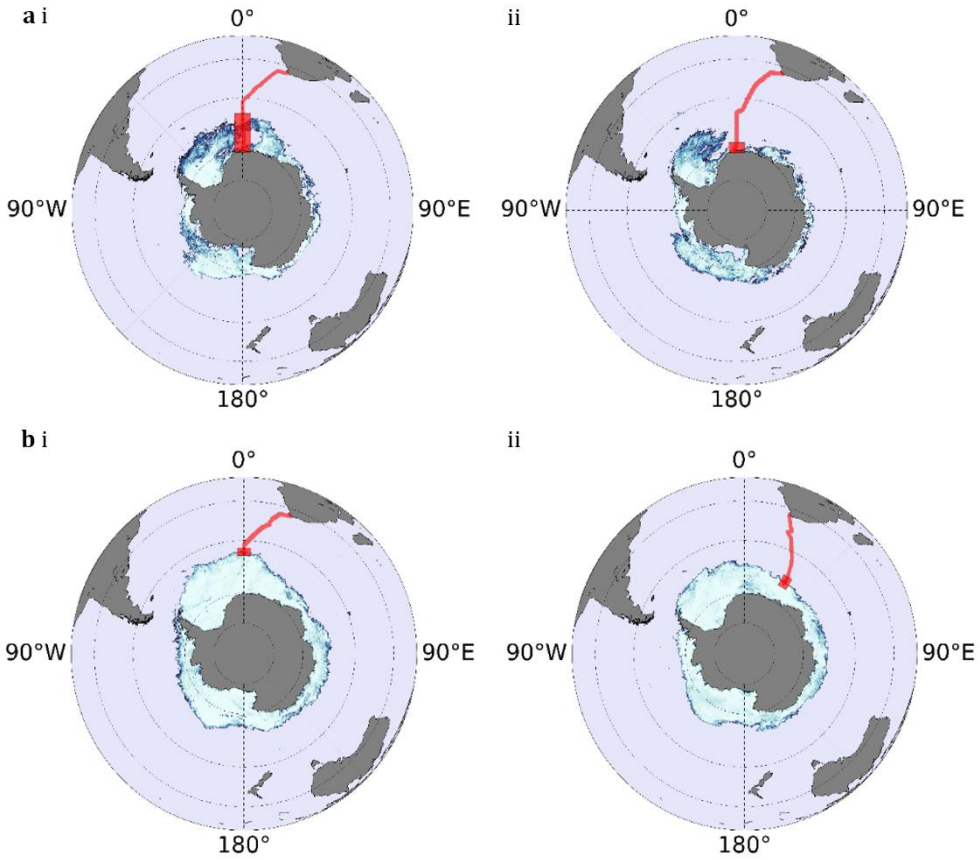

Figure 2.7: Polar stereographic ASI-AMSR2 satellite image (3.125 km grid resolution) of SIC (%) covering the Southern Ocean around Antarctica on the days that the *S.A. Agulhas II* first reached the ice edge during (a) each summer expedition on (i) 07 December 2016 and (ii) 18 December 2017, and during (b) each winter expedition on (i) 21 July 2016 and (ii) 04 July 2017. Overlaying the SIC is the ship track (red line) as well as the studied area of ship-based observations (highlighted box).

As detailed in Section 2.1, hourly ship-based observations were made while the ship sailed through the sea ice environment. From this information, a co-location method was established: where the SIC obtained from the ship was compared against the SIC estimated from PM data within the same location, defined by a grid cell (refer to Figure 2.4). This method was adapted from Beitsch et al. (2015). Figure 2.8 details this co-location method.

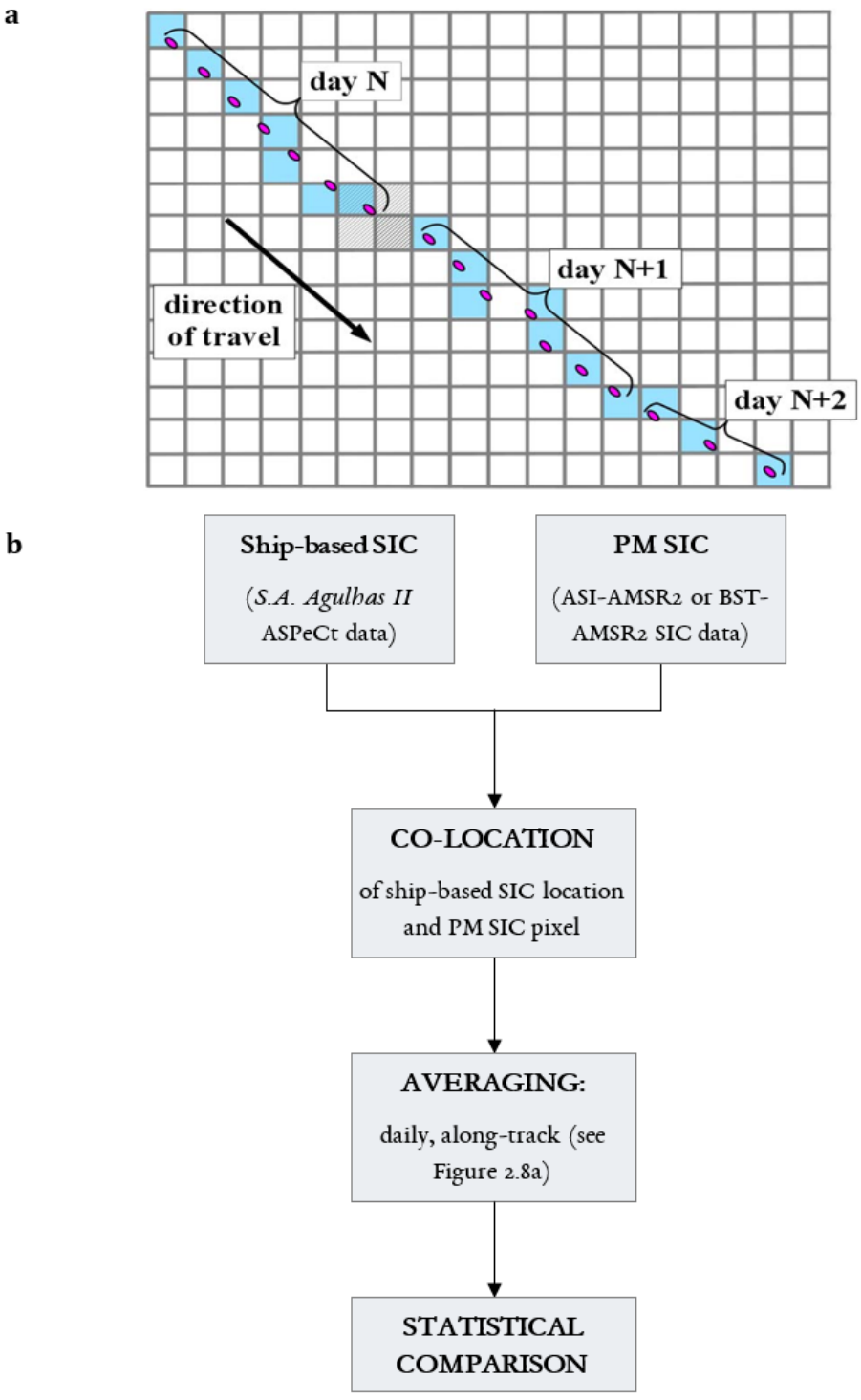

Figure 2.8: A schematic of (a) the co-location method (source: Beitsch et al., 2015). Blue-coloured pixels depict the selected PM grid cells. Pink dots depict the ship points for ship-based SIC observations, and (b) the analysis structure of the co-location method depicted in flow chart form. (Adapted from Beitsch et al., 2015).

As depicted in Figure 2.8, the co-location of the satellite SIC with ship-based SIC was as follows: both PM-estimated SIC was transformed onto a Cartesian grid (e.g.

Figure 2.4), and for each ship-based SIC observation location, the nearest PM-estimated SIC grid cell was computed and their respective SIC values were extracted. In addition to this co-location method, the location of the MIZ edge (at 15% SIC (Meier and Stroeve, 2008, as cited in Chapter 1)) was identified. This identification was achieved through observation, i.e. when the SIC was 15%. However, in addition to this, the observed SIC needed to remain above this 15% mark for at least 1 degree of latitude, and the ship needed to follow a path that was geometrically correct. This geometrically correct pathway meant that the ship needed to travel perpendicular to the ice edge. The co-location and MIZ edge-location results are presented in Sections 3.1.1 and 3.1.2.

Each algorithm's SIC retrieval ability (within the MIZ) was assessed against ship-based SIC using a statistical comparison method detailed by Taylor (2001). Using the cosine rule, this method provides complementary statistical information, such as the root-mean-square difference (RMSD) and the correlation coefficient, which provides quantification of the correspondence between two datasets. For this study, these datasets are satellite and ship-based SIC. Furthermore, for a more complete characterization of the studied area, the standard deviations of the retrieval methods were provided. With this statistical comparison, a Taylor Diagram was constructed (Section 3.1.3) which statistically quantified the degree of similarity between the ship-based observations (the 'reference' field) and the ASI- and BST- AMSR2 estimates (the 'test' fields) (Figure 2.9).

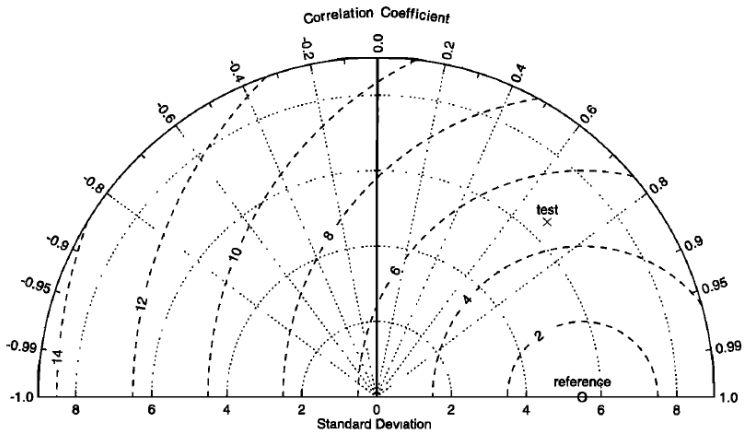

Figure 2.9: Example of a Taylor Diagram for displaying pattern statistics (source: Taylor, 2001).

Figure 2.9 provides an example of a Taylor Diagram. The radial distance from the origin is proportional to the standard deviation (units in %) of a pattern. The centred RMSD between the satellite estimates and the ship-based observations was proportional to their distance apart. The azimuthal position provided the correlation between the two fields. If the 'test' output (the SIC retrieved from PM products) lies close to the 'reference' field (ship-based SIC estimates), the data retrieved generally agrees well with the reference data (detailed in depth by Taylor (2001)).

There are, however, limitations inherent with the data used which has an effect on using this method to test statistical significance. For example, although ship-based observations were conducted hourly, the ASI- and BST- AMSR2 SIC was averaged daily: polar orbiting occurs twice per day and the SIC retrieved from each overpass was combined into one PM SIC value per grid cell (see Figure 2.4). Furthermore, the retrieved ASI- and BST-SIC values represent sea ice conditions on a scale on the order of 3.125 km and 12.5 km, respectively, whereas the ship-based observations were approximately estimated within a 1 km radius. In addition to these spatial and temporal differences, this method can only consider the low frequency of ship-based observations taken within a relatively small area. This study is biased towards a specific area; the Atlantic sector.

2.4 Automatic Acquisition of Sea Ice Concentration

The purpose of this section is to provide a detailed summary of the design and technique to automatically acquire SIC to maximize the retrieval of SIC from cruises not specifically dedicated to sea ice observations.

2.4.1 Image Acquisition

Section 2.1 has introduced a camera set up methodology to support ASPeCt ice observations. The camera's FOV (see Section 2.1.2 and in Figure 2.3b) as well as the algorithm's sea ice identification methodology is detailed in this section.

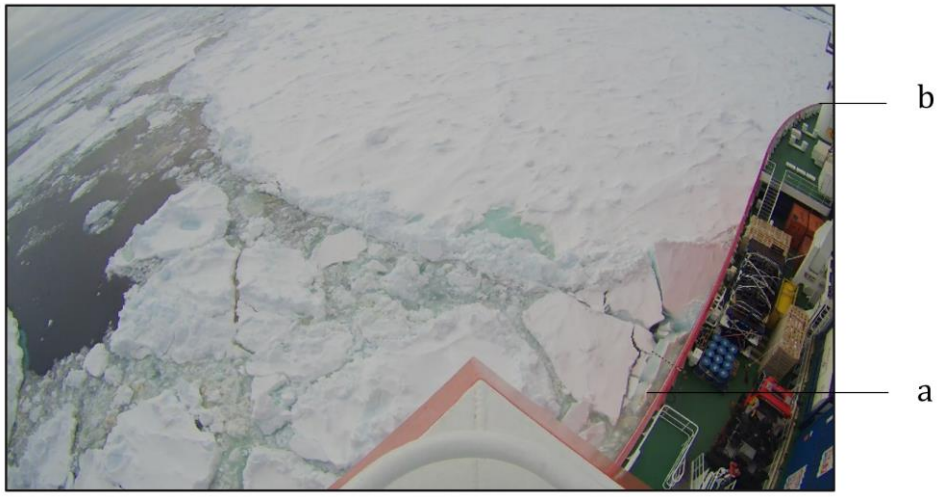

Figure 2.10: The camera's total FOV providing the (a) view of overturning ice floes, and (b) the edge of the hull.

The cameras used for this study were high resolution, off-the-shelf TomTom video cameras with weatherproof casing (Figure 2.3a). The positioning of the camera (detailed in Section 2.1.2) provides a nadir view of the sea ice field which includes overturning ice blocks (a), and the edge of the hull (b) (Figure 2.10). Since this method is designed to retrieve SIC automatically from vessels of opportunity, the details of the camera setup are not important. What is important is that when the camera is set up, the height, angle and FOV must remain the same throughout the expedition.

The areal extent of the FOV defined for this study (Figure 2.10) was decided upon based on a similar study conducted by Weissling et al. (2009). The camera's position provided a port bow FOV. This included the far field image edge slightly above the horizon and the top right image edge comprised of a section of the port side of the hull for reference. This defined FOV was selected due to the wide-angle view coinciding with the view of the ASPeCt observers from the bridge (see Figure 2.2).

2.4.2 Video Pre-Processing

The following pre-processing method was derived from Weissling et al. (2009). The ice field was recorded at 1 second intervals, this included time as well as latitudinal and longitudinal ship position. The recorded rate was chosen to provide continuous coverage of the sea ice conditions. These video recordings were converted from MP4

format files to JPEG images stills through FFMPEG software (downloaded as freeware online: https://www.ffmpeg.org/download.html).

2.4.3 Sea Ice Identification

Due to the camera set-up specific to this study (Figures 2.3 and 2.10), each image provided an oblique view of the sea ice field. To reduce this geometric distortion (which increases with distance from the ship), an uncorrected sub-scene was selected (Figure 2.11a) and defined to exclude the horizon and any portion of the vessel (Figure 2.11b).

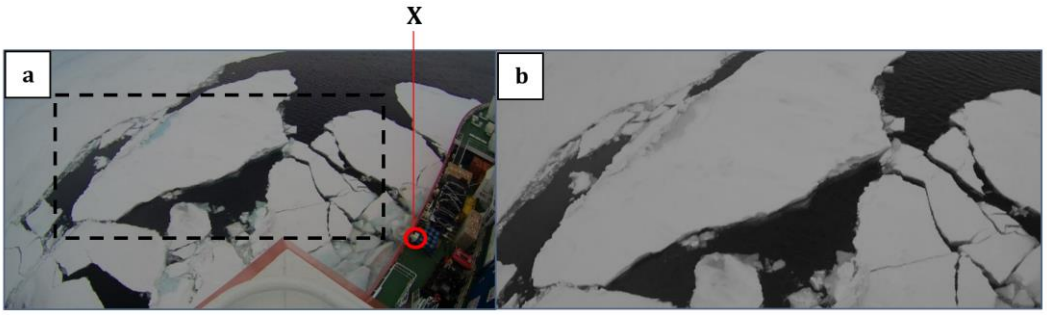

Figure 2.11: The (a) total FOV of the camera, including the highlighted sub-scene, with the (b) extracted grey-scale subscene. Point X marks the brightness reference point.

These sub-scene images showed the sea ice freeboard as a bright, white object against the darker ocean waters (Figure 2.11). Therefore, the pixel values differed under standard conditions and, from the extracted sub-scene images, a grey-scale version was created (Figure 2.11b). This allowed for a set of sub-scene images from which a threshold filter was applied to discriminate white ice from its darker background. The threshold limit was automatically determined using a brightness reference specific to the original image. point X, on Figure 2.11a, shows the pixel location which was used as the brightness reference. This worked based on reference point X changing in brightness as the angle of the sun changed with reference to the ship. This was important as the relative positioning of the sun continuously changed as a result of the ship's direction continuously changing, as well as the change in the time of day. Equation 2.1 details the conversion of grey-scale images to binary images based on the threshold method:

$$\begin{aligned} \text{If } P \geq X &\longrightarrow P = 1 \\ \text{If } P < X &\longrightarrow P = 0 \end{aligned} \qquad [2.1]$$

If a pixel, P, in the grey-scale sub-scene was greater than or equal to the reference pixel, X, the pixel was defined as 'one'. Conversely, if the pixel was less than the reference pixel, 'zero' was defined.

Figure 2.12: Final image showing sea ice (yellow) and water (purple) pixels.

Each pixel equal to one or zero was defined as ice or water, respectively, and a new sub-scene image was created (Figure 2.12); where the yellow pixels were representative of ice, and water was represented by purple. The algorithm would then calculate how many yellow pixels are present in relation to purple pixels, thus providing automatically acquired SIC values within a given time and location.

3 Results

The results are presented as follows: first, in Section 3.1, a comparative analysis is presented between SIC obtained from ship-based and PM data using the co-location method presented in Section 2.3. Following this analysis, the SIC automatically acquired (using the threshold method presented in Section 2.4) is compared against ship-based observations (Section 3.2). Lastly, the seasonal variability of the MIZ SIE (calculated from satellite data) was analysed with respect to the total SIE for the Atlantic sector (Section 3.3).

3.1 Co-Location and Comparison Results

The relationship between the PM-SIC and ship-based SIC observation estimates were assessed using the co-location and comparison methods (Section 2.3). These assessments were conducted using the South African 2016 and 2017 summer (December) and winter (July) Antarctic expeditions as case studies.

3.1.1 Case Study I: Summer 2016 and 2017

During the *S.A. Agulhas II* December 2016 expedition within the MIZ (07.12.2016 – 10.12.2016), 82 ship-based SIC observations were conducted (Figure 3.1a). The ship track is detailed in Figure 2.7a (Section 2.3). The minimum and maximum air temperatures were recorded between -4.8 °C and -2.2 °C, respectively, and the wind speed between 3.60 $m\,s^{-1}$ and 14.10 $m\,s^{-1}$ (approximately 7 to 27 knots). During the December 2017 expedition, 20 ship-based SIC observations took place on 18.12.2017 (Figure 3.1b), recording air temperatures and wind speeds ranging between -3.9 °C – -1.6 °C, and 2.5 $m\,s^{-1}$ – 17.9 $m\,s^{-1}$ (approximately 5 to 35 knots), respectively. The weather

within the MIZ, during both expeditions, was relatively calm, with neither big swells nor heavy snow storms.

Figure 3.1 presents the area in which the summer sea ice conditions were studied and details the SIC observation differences between the AMSR2 PM- and ship-based-SIC estimates.

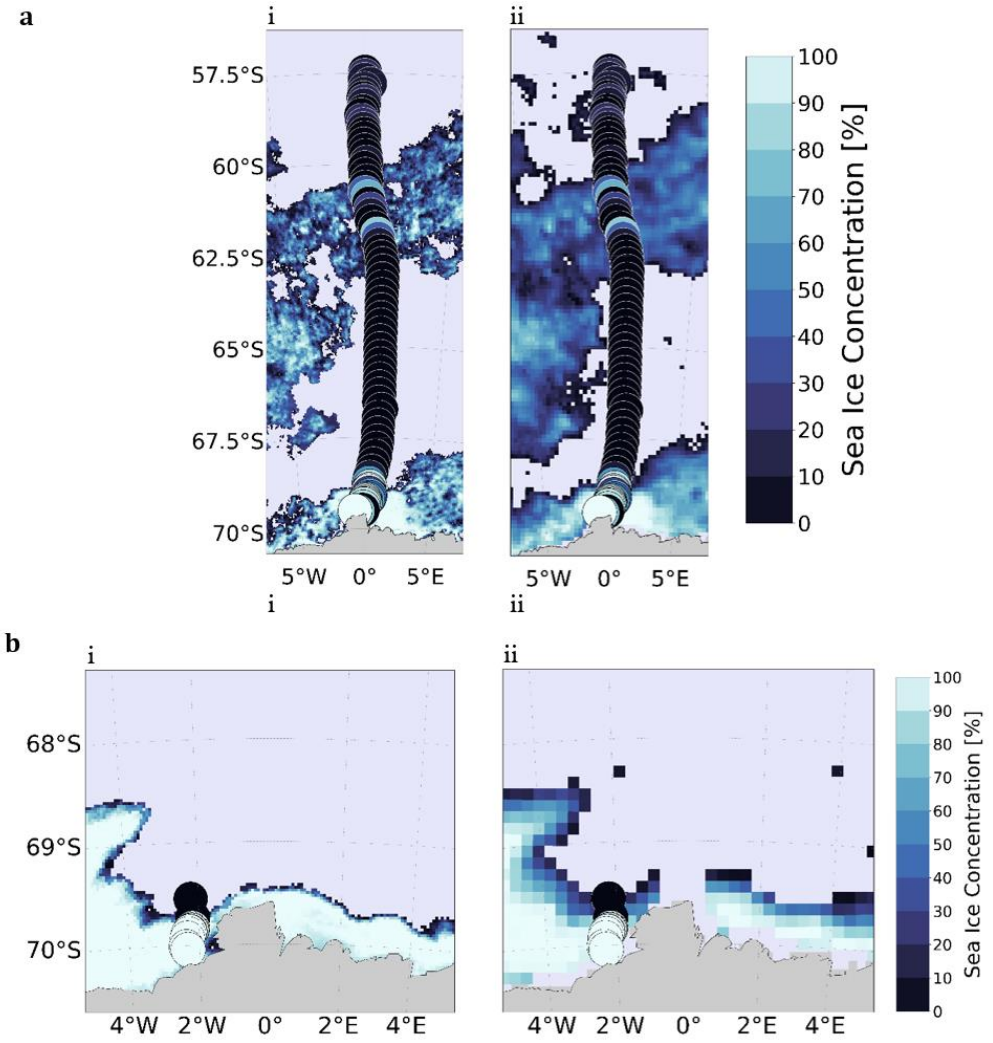

Figure 3.1: SIC (%) from the austral summer ship-based observations (colour-coded points) retrieved from (a) 07-10 December 2016, and (b) 18 December 2017. Overlaid on AMSR2 (i) ASI-AMSR2 (3.125 km grid-resolution), and (ii) BST-AMSR2 SIC (12 km grid-resolution) retrievals on (a) 07 December 2016, and (b) 18 December 2017.

The colour-coded dots in Figure 3.1 show the SIC estimated from aboard the *S.A. Agulhas II* and how these estimations compare against SIC derived from the ASI (Figure 3.1i) and BST (Figure 3.1iii) algorithms. This comparison elucidates the difference in SIC

recoveries using algorithms with different grid resolutions. It is made clear that, relative to the ASI- AMSR2 (3.125 km grid-resolution), the BST- AMSR2 (12.5 km grid-resolution) shows larger patches of low SIC further north. This is emphasized in Figure 3.1a where the BST- AMSR2 product presented low SIC conditions approximately 2.5° (~ 278 km) further north relative to the ASI- AMSR2. Furthermore, this figure shows that the ship-based SIC estimates start slightly further north, estimating patches of low SIC between 10% and 20%. These differences are emphasized in the December 2016 expedition. A more in-depth analysis of the difference in SIC (between the ASI-, BST-, and ship-based-SIC estimates) is presented in Figure 3.2.

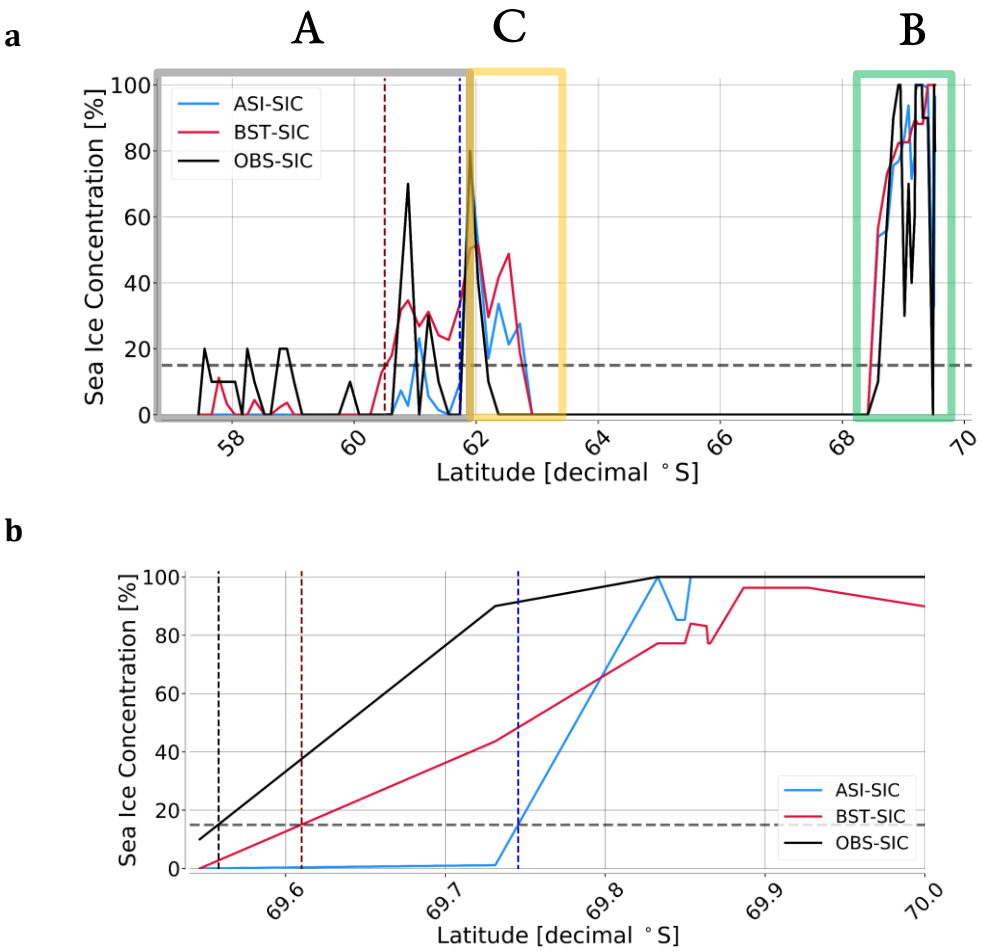

Figure 3.2: SIC (%) retrieved from the *S.A. Agulhas II* Antarctic summer (a) 2016, and (b) 2017 expeditions, estimated using ship-based (OBS-SIC; black line), the ASI-AMSR2 (ASI-SIC; blue line), and the BST-AMSR2 (BST-SIC; red line) observations, with respect to Latitude (decimal degrees). The 15% MIZ edge (horizontal, grey, dotted line) is included, along with the latitudinal location of the 15% OBS-, ASI-, and BST-SIC MIZ edge (black, red, and blue vertical lines, respectively).

Figure 3.2 compares SIC from visual observations against satellites with different grid resolutions. It is observed that the December 2017 MIZ expedition (Figure 3.2b) was characteristically different to the December 2016 expedition (Figure 3.2a). As seen in Figure 3.1, these differences included: a lower frequency of SIC observations in 2017 (4x lower than the observations conducted in 2016), as well as observations taking place closer to the Antarctic continent (where SIC remains relatively high and is classified as pack ice). The lower number of observations and higher SIC conditions meant that the SIC recorded during December 2017 was relatively simple to analyse. Therefore, although Figures 3.1 and 3.2 are displayed according to time sequence, we shall first analyse December 2017.

In 2017, the estimated average of the satellite 15% MIZ edge was approximately 13 km more south relative to the ship-based observations (Figure 3.2b). The analysis of the December 2016 MIZ observations was not as straightforward. Due to a large polynya (a non-linear shaped opening of open water enclosed by sea ice), this observation period was divided into three Sections: Sections A and B, entering the MIZ, and Section C, exiting the MIZ (Figure 3.2a).

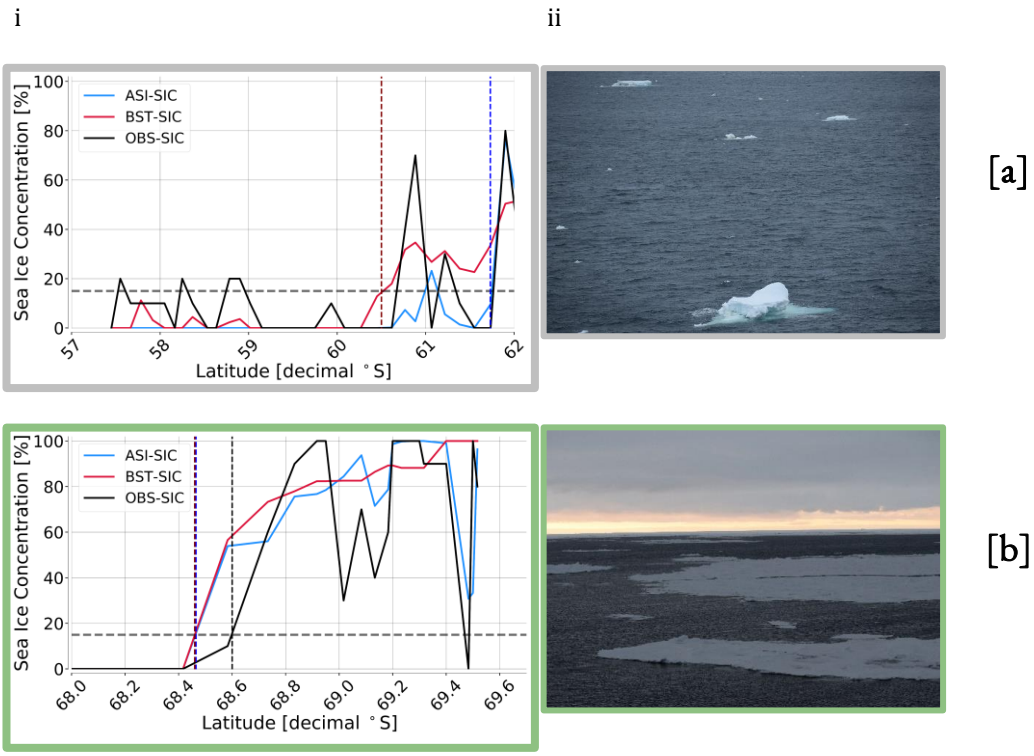

Figure 3.3: First column (i): Ship-based (OBS-SIC; black line), the ASI-AMSR2 (ASI-SIC; blue line), and the BST-AMSR2 (BST-SIC; red line) estimates (%), with respect to Latitude (decimal degrees). SIC retrieved during (a) the first encounter of sea ice, and (b) after exiting the polynya. The 15% MIZ edge (grey, dotted line) is included, along with the latitudinal location of the 15% OBS-, ASI- and BST-SIC MIZ edge (black, red and blue vertical lines, respectively). Second column (ii): images taken off the *S.A. Agulhas II* at the MIZ edge.

As seen in Figure 3.1a, the ship entered MIZ conditions twice; the first time was at 57˚33' S and the second at 68˚16' S. Figure 3.3a shows that when the ship first encountered sea ice, very low SIC was evident through ship-based and BST- AMSR2 estimates (Figure 3.3ai). These estimates included sporadic sea ice conditions of melting ice floes (Figure 3.3aii.). After retrieving these sporadic low SIC conditions, the estimated MIZ edge from the BST algorithm was at 60˚30' S and, thereafter, recorded a gradual increase in SIC (Figure 3.3ai). Relative to this, the ASI- AMSR2 indicated that the MIZ edge was approximately 126 km further south (at 61˚43' S). Interestingly, during these conditions, the location of the 15% ship-based MIZ edge was not defined due to the absence of SIC values greater than 15% for at least a distance of 1-degree latitude (Figure 3.3ai).

Figure 3.1B shows when the ship entered MIZ conditions a second time but closer to the Antarctic continent. The three methods used to obtain ice concentration estimated the MIZ edge at similar latitudes (specifically the ASI- and BST- AMSR2

estimates (Figure 3.3bi)); where larger ice floes were observed (Figure 3.3bii). It was noticed that the satellite products derived the MIZ edge at similar latitudes when the ice floes were larger (Figure 3.3b) compared to when they were relatively smaller (Figure 3.3a).

i ii

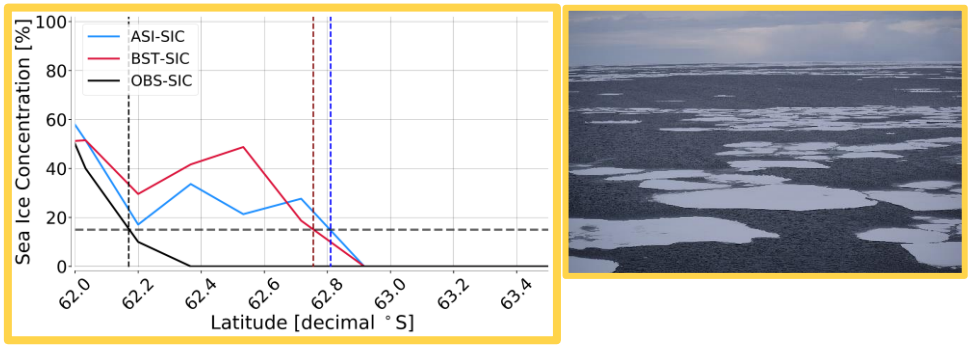

[c]

Figure 3.4: First column (i): Ship-based (OBS-SIC; black line), the ASI-AMSR2 (ASI-SIC; blue line), and the BST-AMSR2 (BST-SIC; red line) estimates (%), with respect to Latitude (decimal degrees). SIC retrieved during (c) the *S.A. Agulhas II* exiting the MIZ edge. The 15% MIZ edge (grey, dotted line) is included, along with the latitudinal location of the 15% OBS-, ASI- and BST-SIC MIZ edge (black, red and blue vertical lines, respectively). Second column (ii): image taken off the *S.A. Agulhas II* of the MIZ edge.

Figure 3.4 shows the difference in SIC estimated between the satellite products and the ship-based observations while exiting the sea ice field (entering the polynya). Both satellite products similarly estimated the location of the 15% MIZ edge. Observing a relatively steep decrease in SIC, the ship-based estimates showed the MIZ edge at approximately 00°35' S (~ 39 km) further north relative to that of the PM products (Figure 3.4i). At this MIZ edge, the predominant ice-type was large and scattered floes (Figure 3.4ii).

3.1.2 Case Study II: Winter 2016 and 2017

The following two case studies were specific to Antarctic winter conditions, focussing on the MIZ SIC recorded in July 2016 (21.07.2016 – 22.07.2016) and 2017 (04.07.2017 – 05.07.2017). The ship track is detailed in Figure 2.7b (Section 2.3).

The 2016 air temperature ranged between at 0.32 °C and 0.74 °C, while the minimum and maximum air temperatures during the 2017 expedition was much lower (-5.70 °C – -2.80 °C). Furthermore, the wind during the 2016 expedition was recorded at speeds from

14.20 – 19.60 m s^{-1} and stronger winds were recorded at 16.00 – 31.00 m s^{-1} during the 2017 expedition. In 2016, moderate snow storms were experienced, and the observations were conducted at night, resulting in poor visibility. These weather conditions were, however, milder in comparison to the conditions experienced during the 2017 expedition; on this occasion a low-pressure system passed over the ship while the visual observations took place. This resulted in heavy snow storms and large swells.

The studied areas, highlighted in Figure 3.5, will be further analysed in Figures 3.6 – 3.8.

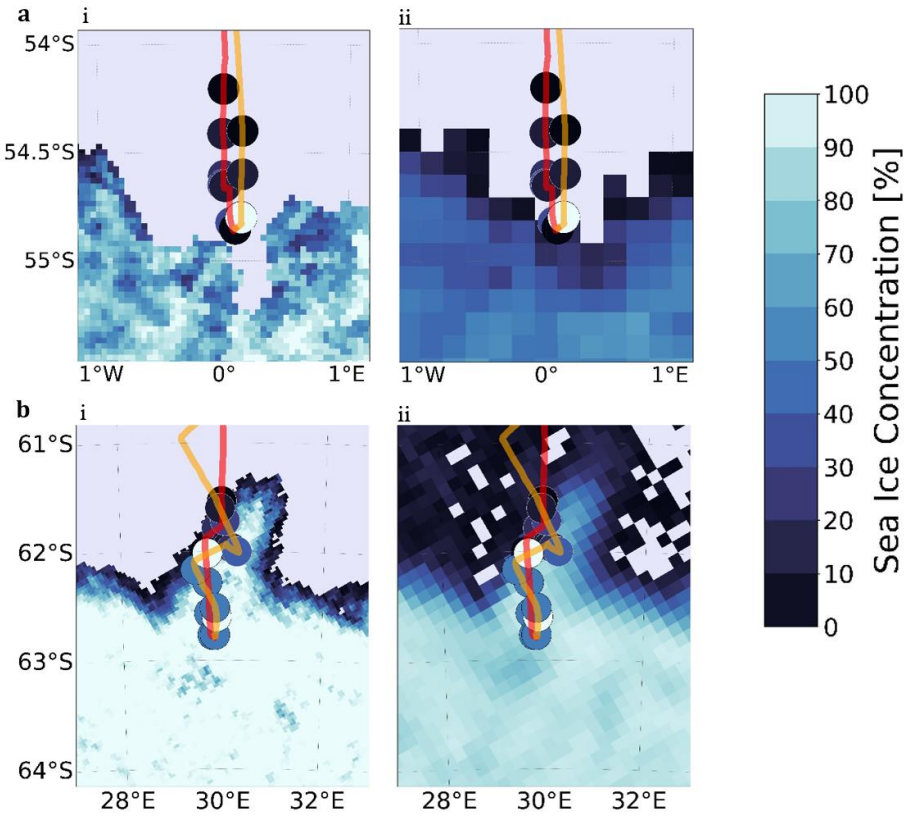

Figure 3.5: SIC (%) from the austral winter ship-based observations (colour-coded points) retrieved from (a) 21 – 22 July 2016, and (b) 04 – 05 July 2017. Overlaid on AMSR2 (i) ASI-AMSR2 (3.125 km grid-resolution), and (ii) BST-AMSR2 SIC (12 km grid-resolution) retrievals on (a) 21 July 2016, and (b) 04 July 2017. The red and orange lines represent the ship entering and exiting the sea ice environment, respectively.

Figure 3.5 demonstrates the difference in SIC from the ship-based (color-coded dots) and PM estimates in winter conditions. During the 2016 winter expedition, the ship travelled within sea ice for approximately 45 km before exiting again (Figure 3.5a). However, the satellite-derived sea ice was over 50 km further south relative to when ice

was first observed aboard the ship (at 54˚24' S) (Figures 3.5a and 3.6a). Therefore, during this expedition, the 15% MIZ edge could not be identified as the ship did not transect the ice for more than a distance of 1-degree latitude and there was also no latitudinal match between visual observations and the satellites.

Figure 3.5b presents the 2017 winter expedition. During this expedition, the ship did not transect the MIZ perpendicularly as it travelled along the MIZ edge due to the shape of the sea ice tongue. Given the sharp changes in sea ice conditions, it was not possible to suggest an approximate location of the 15% MIZ edge and, therefore, a comparison was not possible. To better understand the MIZ SIC recovery differences, an in-depth analysis is provided in Figures 3.6 and 3.7.

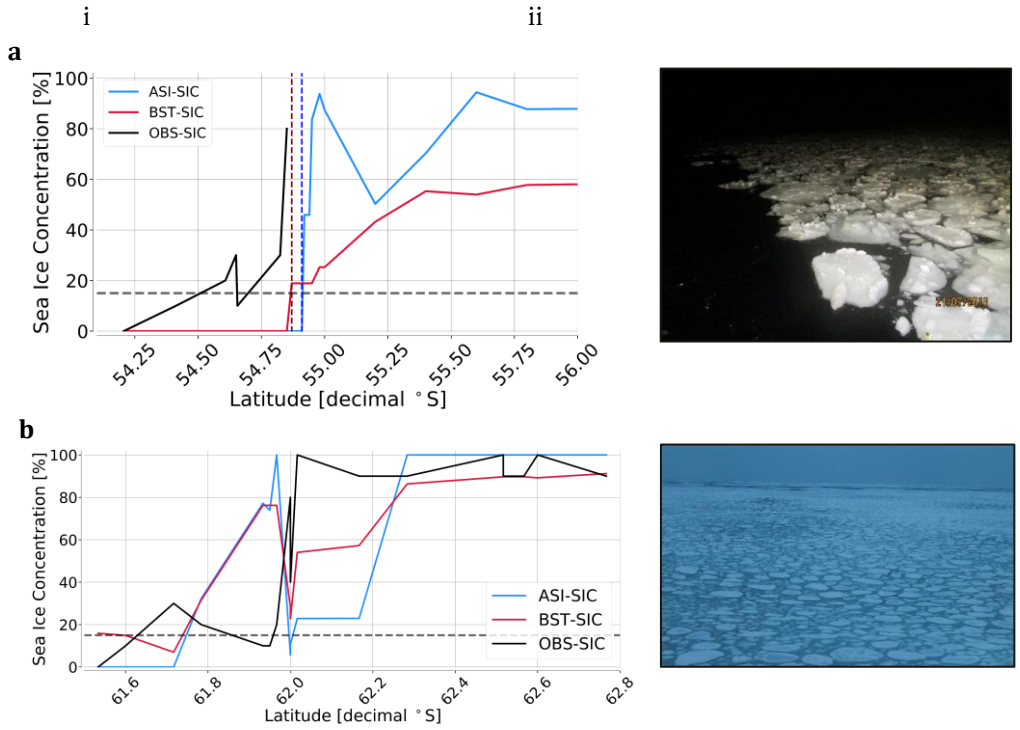

Figure 3.6: First column (i): SIC (%) retrieved from the *S.A. Agulhas II* Antarctic winter (a) 2016, and (b) 2017 expeditions; estimated using ship-based (OBS-SIC; black line), the ASI-AMSR2 (ASI-SIC; blue line), and BST-AMSR2 (BST-SIC; red line) observations, with respect to Latitude (decimal degrees). The 15% MIZ edge (horizontal, grey, dotted line) is included, along with the latitudinal location of the 15% ASI- and BST-SIC MIZ edge (red and blue vertical lines, respectively). Second column (ii): image taken off the *S.A. Agulhas II* of the respective winter MIZ edges.

During both winter expeditions, the ship entered the MIZ and, several hours later, exited it (Figure 3.5). Because of the ship transecting the MIZ southward as well as northward, the latitudinal points needed to be reorganized in ascending order (Figure 3.6). Ship-based observations recorded a rapid increase from 15% to 90% SIC in the space of approximately 45 km during 2016, and during 2017, an increase from 15% to 100% SIC was observed in the space of approximately 27 km. Even though 90% and 100% SIC was recorded, the ship never crossed pack ice conditions as only sea ice conditions characteristic of the MIZ was observed (i.e., frazil and brash ice located in between pancake ice). Figure 3.7 shows the MIZ at 90% and 100% for both 2016 and 2017 winter expeditions, respectively.

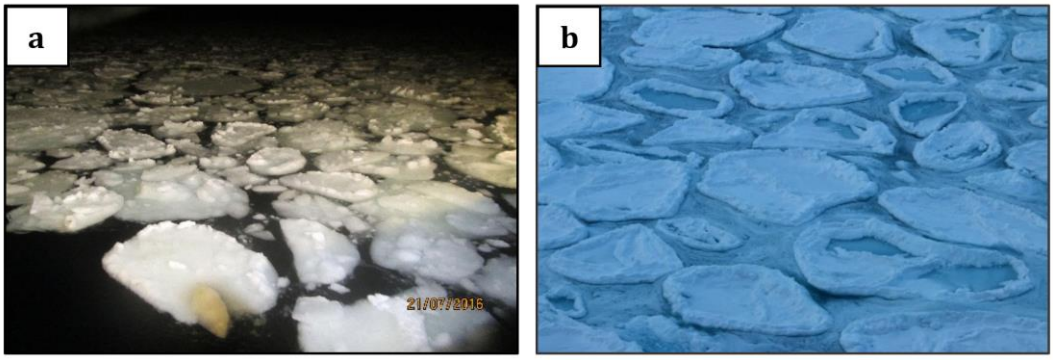

Figure 3.7: Images showing the high MIZ SIC (%) captured aboard the *S.A. Agulhas II* during the winter (a) 2016 (90% SIC), and (b) 2017 (100% SIC) expeditions.

As observed during the winter 2017 expedition, the MIZ environment was dominated by a combination of frazil and brash ice located in the interstices between the individual pancakes (Figure 3.7b). Interestingly, there was no frazil ice observed during the winter 2016 expedition (Figure 3.7a). It was further observed aboard the ship in 2017 that high wind and wave energy prevented the frazil ice from congealing into coherent sheets for hundreds of kilometres inside the MIZ edge (as cited by Doble et al., 2003, and Kohout et al., 2014 in Chapter 1).

3.1.3 Statistical Analysis

Table 3.1 summarizes the comparison between the AMSR2 satellite products and the ship-based observations (see Sections 3.1.1 and 3.1.2) through the correlation coefficient, the RMSD, and the standard deviations (see Section 2.3).

Table 3.1: Statistical summary of the relationship between the ASI- and BST-AMSR2 SIC estimates and the ship-based SIC observations (OBS).

	Summer 2016		Summer 2017		Winter 2017	
	ASI-AMSR2	BST-AMSR2	ASI-AMSR2	BST-AMSR2	ASI-AMSR2	BST-AMSR2
Correlation Coefficient	0.87	0.84	0.75	0.90	0.44	0.57
Standard deviation (%)	35	35	35	25	43	31
	OBS=34		OBS=24		OBS=38	
RMSD (%)	17.66	19.45	23.71	10.71	43.13	32.68

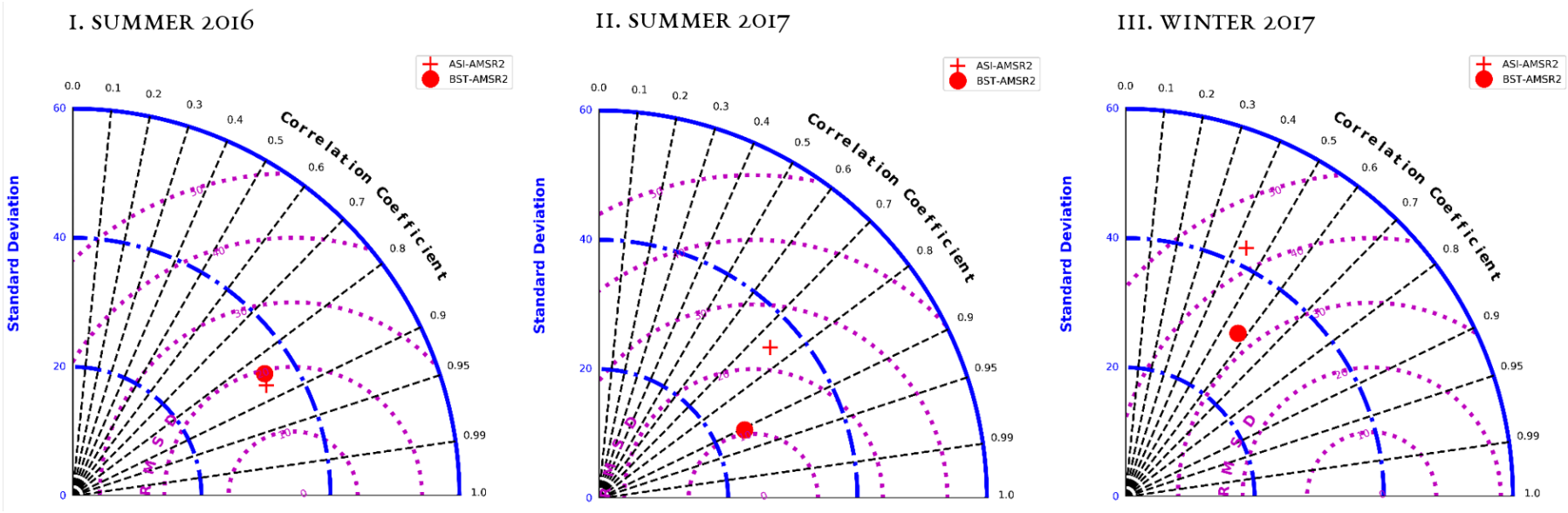

Figure 3.8: Taylor Diagrams showing the relationship between the ship-based SIC observations with the ASI-AMSR2 and BST-AMSR2 SIC estimates for the (i) summer 2016, (ii) summer 2017, and (iii) winter 2017 South African Antarctic expeditions.

Using the statistical values presented in Table 3.1, Figure 3.8 details the comparison between each SIC retrieval method using the Taylor Diagram (detailed in Section 2.3). For summer 2016, the ASI- and BST-AMSR2 products were highly correlated (0.87 and 0.84, respectively) with the ship-based estimates (standard deviations = 35% while that of the ship-based observations = 34%). Furthermore, both PM products had a relatively low RMSD. With the few observations obtained from the summer 2017 expedition, it was concluded that the BST-AMSR2 product was highly correlated with ship-based observations (0.90) with a similar standard deviation (25%) to the ship-based standard deviation (24%). Furthermore, the RMSD was much lower relative to the ASI- AMSR2 product which had a relatively lower correlation (0.75) and higher standard deviation (35%).

A statistical analysis could not be completed for the winter 2016 expedition, as there was no latitudinal match between observations and the satellites (Figures 3.5a and 3.6a; as discussed in Section 4.1). For the winter 2017 expedition, the correlation was substantially lower than the correlations observed between the PM products and ship-based observations in both summer expeditions. For example, during winter 2017, the ASI- and BST-AMSR2 products have a much lower correlation of 0.44 and 0.57, respectively. However, the BST-AMSR2 product was closer to the ship-based observations relative to the ASI-AMSR2 product.

3.2 Automatic Acquisition of Sea Ice Concentration

Ship-based SIC estimates are, in summary, highly variable due to the subjective bias of human interpretation of the sea ice environment (Section 2.1.3). To correct for and to assess this bias in an objective way, an algorithm was developed to automatically acquire SIC (see Section 2.4).

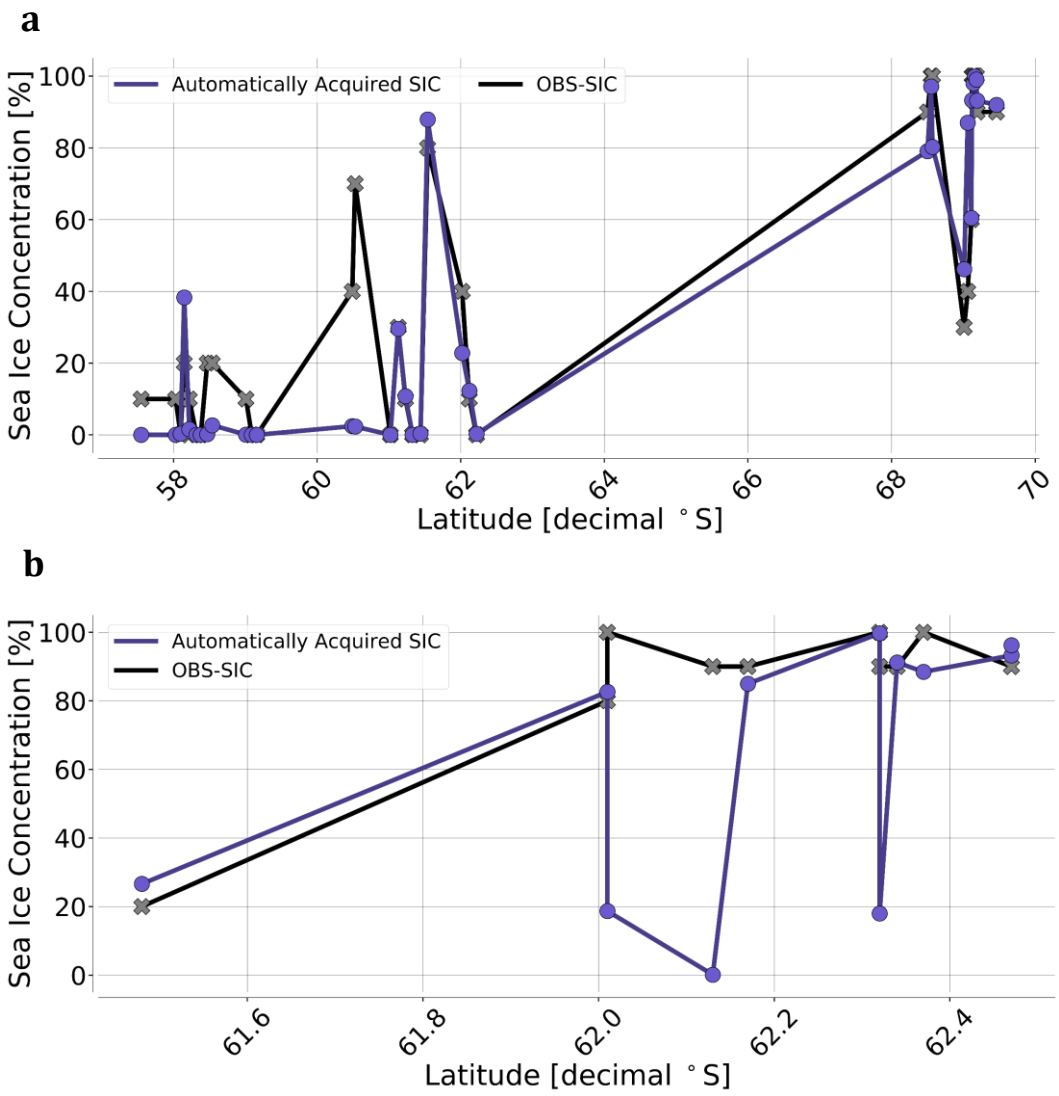

Figure 3.9: SIC (%) retrieved along latitude (decimal degrees) from ship-based (OBS-SIC; black line), and the algorithm designed to automatically acquired SIC (purple line) for (a) the summer 2016 and (b) the winter 2017 expeditions aboard the *S.A. Agulhas II*.

Figure 3.9 presents the difference in SIC obtained from visual observations and video recordings from the *S.A. Agulhas II*. The analysis of the videos was done for summer 2016 and winter 2017, in which the MIZ was approximately between 57.5 – 69.5 °S and 60.5 – 62.5 °S, respectively. Figure 3.9a shows that during summer, the automatic SIC estimates from the videos correlated relatively well with the ship-based observations (correlation coefficient = 0.68). Interestingly, for this summer expedition, the automatic algorithm correlated very well within the MIZ (61.0 – 69.5 °S; correlation coefficient = 0.88), but when the sea ice was first encountered (between 57.5 and 61.0 °S) there was a

much lower correlation of 0.48. Therefore, in summer, the algorithm worked better deeper into the MIZ than at the beginning of it.

During the winter expedition, there was a much larger discrepancy between the two methods (correlation coefficient = 0.29) (Figure 3.9b). The methods were out of phase at the beginning of the MIZ and, deeper into the MIZ, the visual observations recorded relatively high SIC (between 80% and 100%) while the algorithm occasionally acquired much lower concentration values of 0% and 20%. Overall, the algorithm worked better in summer than it did in winter (as discussed in Section 4.2).

3.3 Antarctic Sea Ice Extent: Seasonal and Inter Annual

The data analysed in the preceding sections have allowed to compare, for the first time, SIC from remote sensing with direct observations in the eastern Atlantic sector. More cruises are needed to achieve full validation, but the satellite data can already be used to derive initial information on the seasonal variability of the Antarctic sea ice. To answer the longer-term scientific question of this study, the seasonal SIE was calculated from ASI-SSMIS SIC estimates (Section 2.2.1) which will allow this section to contrast the seasonality in the Atlantic sector with the entire Southern Ocean.

Figure 3.10 compares the climatological seasonal cycle over the period 1981 – 2010 with the recent anomalous years 2016 and 2017.

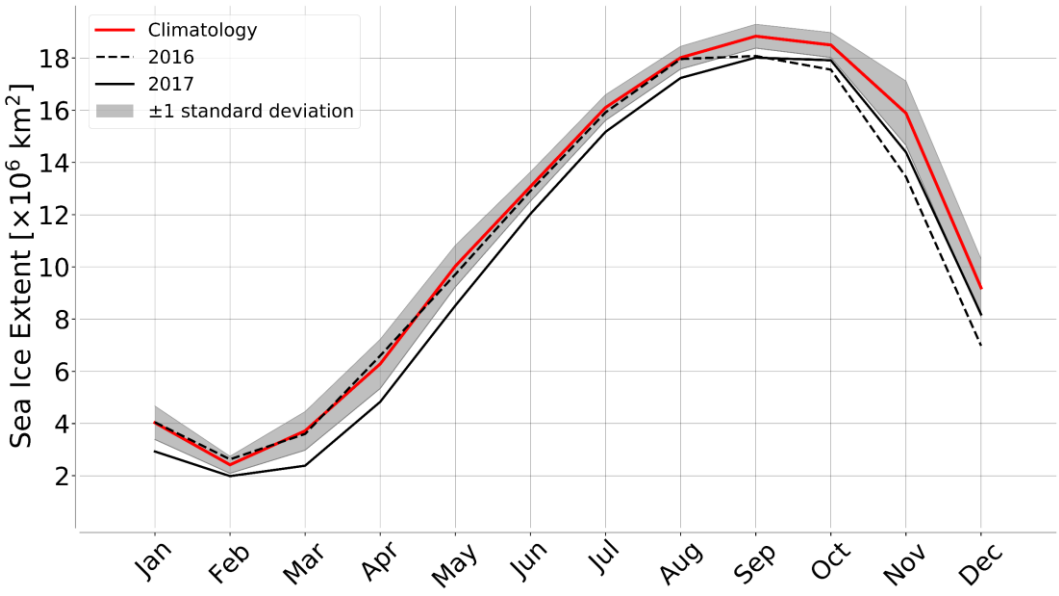

Figure 3.10: Daily Antarctic sea ice extents for the climatology (1981 – 2010; red line), 2016 (dotted black line) and 2017 (solid black line).

These recent 2016 and 2017 anomalous years were first reported by Turner et al. (2017). From January until August, the 2016 SIE was similar to the climatology. However, from early-spring to early-summer (September – December) SIE values were lower by 9%. The year 2017 showed the lowest SIE values throughout the year (8% lower than the climatology), and, from January until early-October, it was 10% lower compared to 2016.

The average SIE was calculated for each month starting from 1997 to 2017 and subtracted from the climatological seasonal cycle, resulting in the seasonal and inter annual SIE anomalies (Figure 3.11). These anomaly results indicate a major shift in SIE during the past two years (2016 – 2017) compared to the past twenty-one years (1997 – 2017) as reported by Maksym (2018) and Turner et al. (2017).

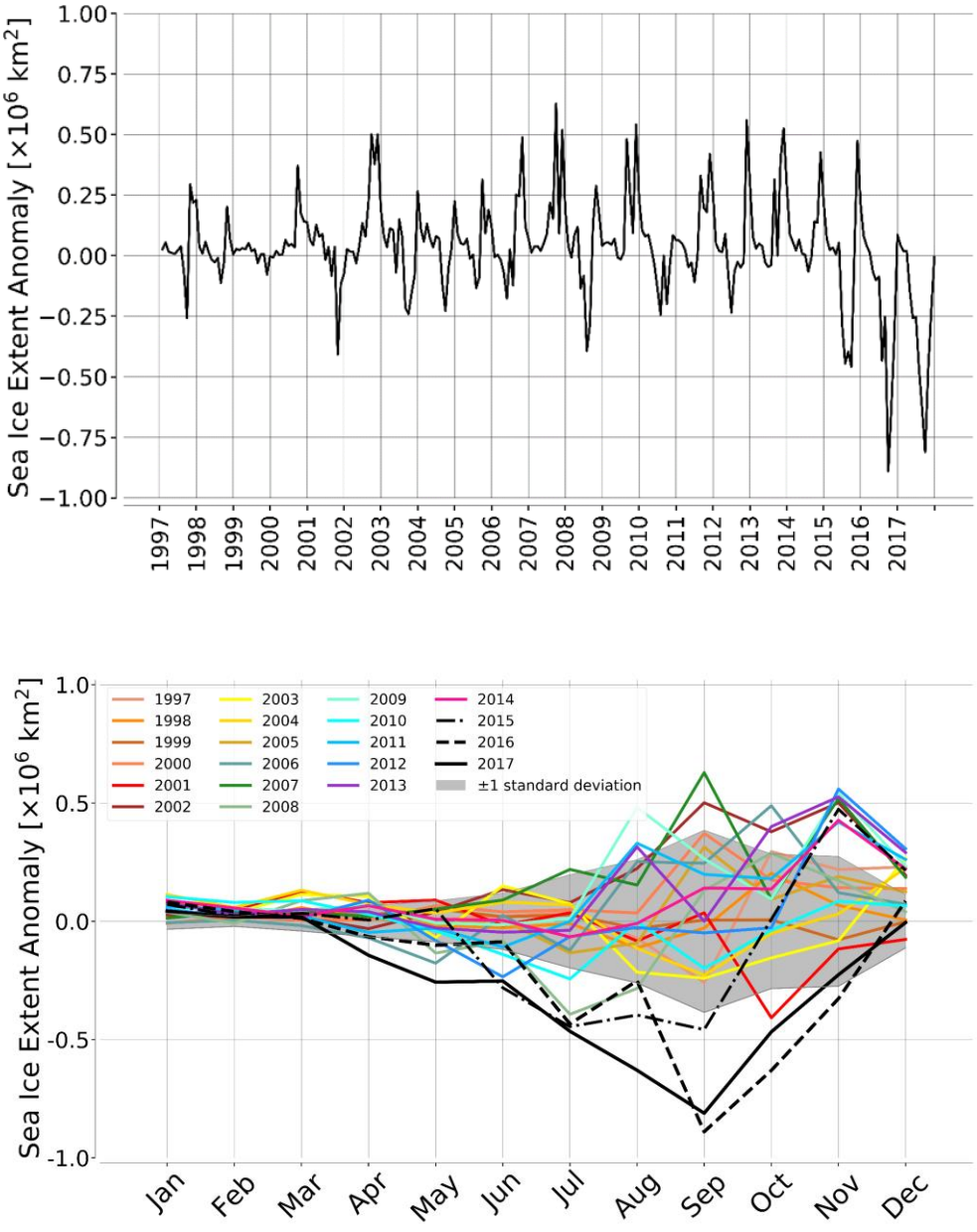

Figure 3.11: Anomalies indicative of the (a) inter annual, and (b) seasonal variation in sea ice extent from the climatology over the past twenty-one years (1997 - 2017). Values are derived from the satellite passive microwave data from ASI-SSMIS.

There were alternating years of anomalously higher and lower inter annual SIE variability from 1997 – 2015. However, 2016 and 2017 showed a precipitous decline in SIE (Figure 3.11a). To gain an in-depth understanding of these results, the seasonal SIE anomaly variability was analysed over each month (Figure 3.11b). This analysis showed that, on average from January through to July, the departure from the long-term mean was similar for several years, although from August to December there was some

variability. The year 2015 showed different seasonal SIE variability which included anomalously low SIE from June – September, but a steep increase in November. Thereafter, substantially low SIE trends were observed from July 2016 through November 2017. During both years, the anomalously low SIE was greatest in September; during this month there was 0.89 x 10^6 km^2 (in 2016) and 0.81 x 10^6 km^2 (in 2017) less SIE than the climatology (Figure 3.11b).

This overall Antarctic SIE, remaining relatively stable from 1997 – 2014 and decreasing through 2016 – 2017, may have masked regional variability. Therefore, we computed the SIE seasonal variability for the Atlantic Sector (Figure 3.12).

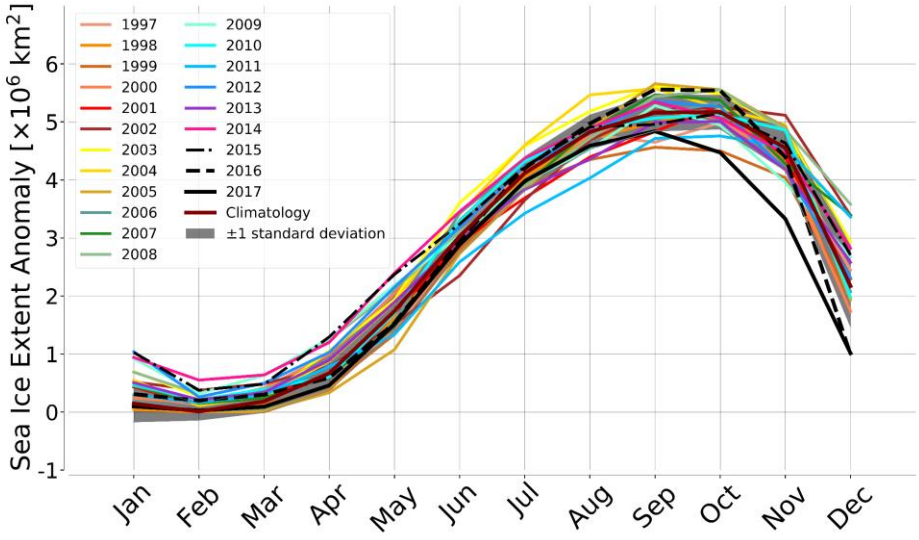

Figure 3.12: Monthly Atlantic Ocean ice extents for the climatology, 2015, 2016, 2017, and averaged over 3-year periods 1997 - 1999 through 2012 - 2014. Values are derived from ASI-SSMIS.

The Atlantic SIE recorded over 2016 and 2017 remained similar to that of the climatology until the early-spring to early-summer months (September – December). In contrast with the Southern Ocean mean SIE (Figure 3.10), the 2016 SIE was, on average, 7% higher than that of the climatology in September and October, and 20% lower from November to December. The year 2017 was always below the climatological mean, although not the lowest year on record. It then showed steep decline from September which continued for the remainder of the year (an average of 20% lower from September – December) (Figure 3.12). Figure 3.13 displays the September spatial variation. We chose

to focus on the month of September because this is when the ice cover reaches its annual maximum extent and when the anomalously low 2016 and 2017 extents were recorded in the Southern Ocean.

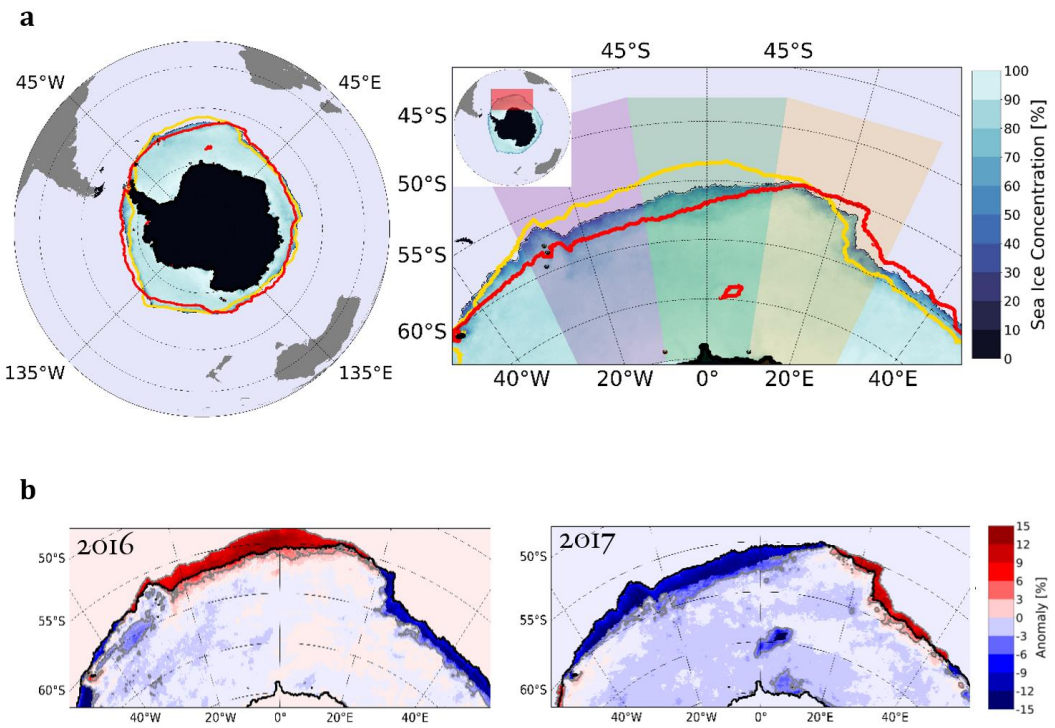

Figure 3.13: (a) The Antarctic MIZ edge from ASI-SSMIS for 2016 (gold contour), and 2017 (red contour), and the SIC for the climatology (colour-coded), when the ice cover reached its annual maximum extent in September. The Eastern Weddell, Lazarev and Riiser-Larsen sectors are highlighted in purple, green and orange, respectively. Included are (b) the September sea ice anomalies from 2016 and 2017.

Figure 3.13a shows the spatial variation of the 15% sea ice edge for 2016 and 2017 in relation to the September climatology, specific to the Atlantic sector. It was noticed that different patterns of SIE variability were observed when compared against the entire Southern Ocean (where 2016 and 2017 reached their precipitously low SIE (Figure 3.11b)). Interestingly, the primary difference within the Atlantic sector was that the 2016 MIZ edge was, on average, further north relative to the 2017 and the climatological MIZ edges (Figure 3.13a). To place in context this Atlantic sector sea ice rise in September 2016 and decline in September 2017, monthly SIC was subtracted from the September climatology resulting in the monthly anomalies (Figure 3.13b). This showed us that, although the September 2016 and 2017 Atlantic extents were, on average, relatively higher and lower

than the climatology, respectively, there was different spatial variation observed in regions within the Atlantic sector. Over 2016, changes in the September ice extent included expanding (red) SIE in the Eastern Weddell and the Lazarev sectors and retreating (blue) SIE in the Riiser-Larsen sector, while 2017 showed opposite patterns (Figure 3.13b).

These anomalies emphasize the importance of studying regional heterogeneity and are highlighted within the MIZ where the SIC does not exceed 80% (Figure 3.3b). Therefore, the seasonal variability of the MIZ in these particular years may elucidate some mechanisms about how the anomalies evolved. We conclude this study by observing the importance of understanding the seasonal variability of the MIZ extent (Figure 3.14).

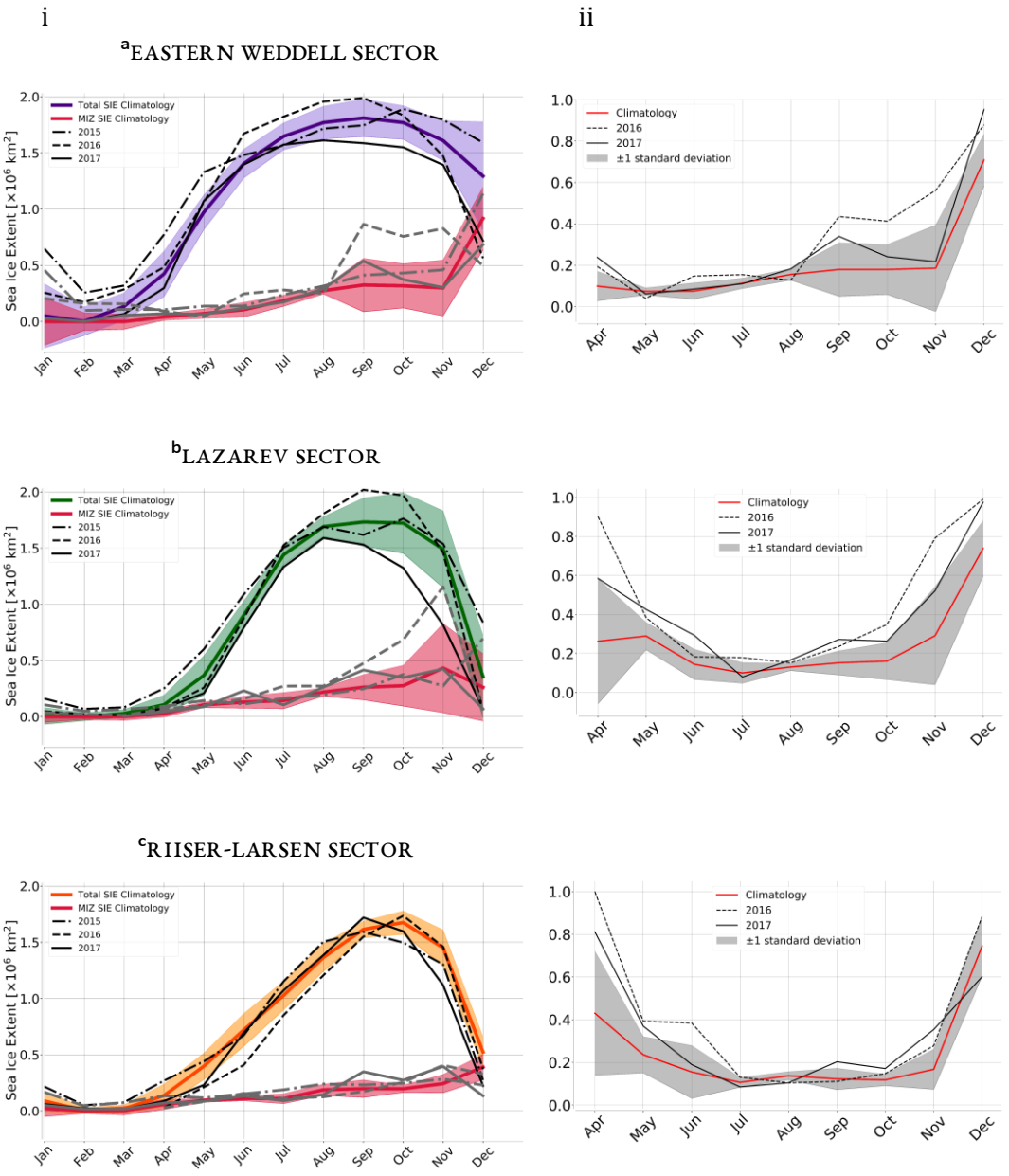

Figure 3.14: The (i) blue and red line present the total SIE (0% - 100% SIC) and the MIZ SIE (15% - 80% SIC), respectively. The (ii) ratio (MIZ SIE/Total SIE) is included. These results are specific to the (a) Eastern Weddell, (b) Lazarev, and (c) Riiser-Larsen sectors.

The Atlantic sector was divided into three separate sectors; the Eastern Weddell (Figure 3.14a), Lazarev (Figure 3.14b), and Riiser-Larsen (Figure 3.14c). Figure 3.13 shows where in the Atlantic these sectors are located. Since the seasonal variability remains similar within the Southern Ocean and Atlantic (with a minimum and maximum SIE around February and September, respectively), the Atlantic sector was divided into three

separate sectors to identify whether this seasonal variability is the same within smaller regions. The first column (Figure 3.14i) shows that the total SIE within each sector has similar seasonal variability to that observed in the Southern Ocean and Atlantic sectors. The MIZ extent (red line) is included in Figure 3.14i to show the seasonal variability of the MIZ (Figure 3.14i). This was done because we observed in Figure 3.13b that anomalous patterns are observed in the MIZ and, therefore, concluded that analysing MIZ variability is important. Figure 3.14i showed that the seasonal cycle of the MIZ SIE was different to that of the total SIE as a gradual increase from autumn to early-summer (March – December) was observed. It is believed that the largest MIZ extent is found in spring (September – November) because, during this time, the ice environment is less consolidated.

In addition to observing the seasonal variability of the total and MIZ extent, their ratio (MIZ SIE/total SIE) was included (Figure 3.14ii). By computing this ratio, the relationship between the total and MIZ extent was better highlighted. It is interesting to notice that if the ratio is above the climatology over the winter months (July – August), the total SIE will show an anomalous decline over the months to follow (September – December) (Figure 3.14ii). Therefore, by focussing on the MIZ SIE in winter, it is inferred that we can approximate what the total SIE might be over spring and summer. We observe this pattern over all Atlantic sectors, but it is emphasized in the Eastern Weddell and the Lazarev sectors (Figures 3.14a and 3.14b).

4 Discussion and Conclusions

The most common technique used when studying the Polar sea ice environment is through using satellites. When studying sea ice seasonal variability using satellite PM estimates, it is important to assess the limitations inherent in PM satellite-derived SIC. Consequently, our aim of assessing the seasonality of the MIZ extent in the Atlantic sector was accomplished by using a three-step approach. Firstly, using a co-location method (see Section 2.3) to conduct an assessment phase by evaluating how well satellite-derived SIC compared against ASPeCt SIC observations from the *S.A. Agulhas II* (Section 3.1). Secondly, by exploring an algorithm to automatically acquire SIC from image stills and videos (Sections 2.4 and 3.2). This second step explored the possibility to augment and improve visual observations in a more objective way. Thirdly, the seasonality of the ice concentration in the MIZ was analysed taking into consideration the knowledge acquired through the *in situ* set of observations.

4.1 The Assessment Phase

It has previously been reported that the total Antarctic SIE has rapidly declined over the years of 2016 and 2017 (e.g. Maksym, 2018), and that studying regional heterogeneity is important (e.g. Comiso et al., 2011; Stammerjohn et al., 2012; Turner et al., 2016). Focussing on 2016 and 2017, this study compared PM-SIC estimates against ship-based SIC observations within the unsampled eastern Atlantic MIZ sector (more specifically, along 0 ° Longitude and 30 ° E). Since satellite data use an operational threshold minimum of 15% SIC (Meier and Stroeve, 2008), we used this threshold to assess the quality of PM satellites. This was done by comparing their ability to estimate the location of the 15% edge against observations collected aboard the *S.A. Agulhas II* (Section 3.1).

We further assessed the satellites against ship-based observations by comparing the SIC values within the MIZ (> 15% SIC).

The statistical analysis, presented in the Taylor Diagram (Figure 2.9), indicated that there was a lower correlation between the ASI- and BST-AMSR2 products and the ship-based estimates in winter (correlation coefficient = 0.44 and 0.57, respectively) relative to summer (mean correlation coefficient = 0.81 and 0.87, respectively) (Section 3.1.3). Therefore, the measurement of sea ice features through PM sensors was more uncertain during winter. This contrasted with results presented by Worby and Comiso (2004) where they concluded that the ship data agreed better with satellite data in the growth season (March – October) relative to the melting season (November – February). This study collected ship-based data within two months (July and December) rather than over several months within the growth and melting seasons. Therefore, this study had a shorter observation period relative to Worby and Comiso (2004) which may be the reason for the discrepancy between the two studies. More South African expeditions are needed to collect more ship-based SIC observations to build a robust comparison between the ship-based and PM SIC techniques. Furthermore, we suggest that the lower correlation between the two methods in winter may be a result of the impact that metocean variables have on SIC estimated through T_b (defined in Section 2.2). However, this study did not go into depth with exploring the impact or uncertainties that arise when using T_b. Therefore, we consider a study conducted by Ivanova et al. (2015) who found challenges associated with surface melt signatures in the T_b data (see Section 2.2.2) which are influenced by metocean variables such as strong wind and waves. These variables are characteristic of storms impacting the Antarctic MIZ environment during winter (as experienced aboard the *S.A. Agulhas II* during both the 2016 and 2017 winter expeditions) (Section 3.2.1). Such metocean variables may cause a disturbance in the sea ice environment, affecting the heterogeneity of the sea ice surface which may weaken the quality of the PM-SIC estimates. An additional variable that may impact the quality of SIC estimates is ice-snow interface flooding which has not yet been quantified for Antarctic sea ice (Stroeve et al. 2016). Petty et al. (2018) found that uncertainties linked to deriving SIC through T_b include challenges associated with open water fractions (an

area of water present within the sea ice environment). During the 2016 and 2017 *S.A. Agulhas II* expeditions, large areas of open water were evident when sea ice was first encountered on the ship (Figure 1.3). It was therefore suggested that the higher SIC estimated through ship observations and the lower SIC recorded from PM at the beginning of every *S.A. Agulhas II* expedition (Figures 3.2 and 3.6) may be due to these large areas of open water.

While being in conditions that were typical of the MIZ, the highest ship-based SIC was recorded at 90% during the winter 2016 expedition and at 100% during the winter 2017 expedition (Figure 3.7). However, because of shortcomings inherent in PM-SIC measurements, the MIZ is defined between two SIC contours: typically, between 15% and 80%. The 15% boundary corresponds to the conventional MIZ edge (Comiso, 2006) and the 80% boundary is defined by the World Meteorological Organization as 'close ice' (WMO, 2009). We suggest that the maximum threshold of 80% SIC is not accurate for PM-SIC estimates within the Atlantic MIZ because SIC higher than 80% was observed in conditions characteristic to the MIZ environment. We further suggest that PM imagery of consolidated pack ice does not necessarily mean compact ice cover. Stroeve et al. (2016) found that the satellite may indicate 100% SIC (e.g., consolidated pack ice) when, in reality, the ice environment is more characteristic of the MIZ (e.g., frazil ice and small ice floes). It is important to note that south Atlantic MIZ expeditions rely on PM SIC imagery to plan for the science conducted onboard and for safe and efficient ship-track navigation. Therefore, should the Atlantic MIZ environment be misinterpreted through analysing PM images, resources such as time, money, and science may be jeopardized. It is important to understand these limitations associated with how the MIZ is operationally defined for future south Atlantic expeditions.

Focussing on the 15% SIC minimum threshold defined for the MIZ edge, it was calculated that, during the summer 2017 expedition, the 15% ship-based MIZ edge was located at 69°33' S and the MIZ edge of the BST- and ASI-AMSR2 products were recorded at 69°36' S and 69°44' S, respectively. This implies that the error of the 15% satellite MIZ-edge estimated location was, on average, approximately 13 km (Figure 3.2).

This is very good as many polar-orbiting satellites have a grid-resolution of 12 - 25 km. When estimating the 15% *in situ* MIZ edge, the ship should record SIC for a distance of at least 1-degree latitude and the ship needs to follow a pathway that is geometrically correct to compare to the satellite (Section 2.3). This geometrically correct pathway means that the ship is required to travel perpendicular to the MIZ edge. This is, however, difficult because the concentration derived using satellite may not be accurate. For these reasons, this estimation of the 15% *in situ* MIZ edge location was provided only for the summer 2017 expedition and not for the summer 2016 expedition. This was because, during the summer 2016 expedition, the ship-based SIC observations were not continuously recorded over 1-degree in latitude. Furthermore, the 15% MIZ edge location for the 2016 and 2017 winter expeditions was not estimated because the former did not transect the MIZ for more than 1-degree latitude (Figures 3.5a and 3.6a), and the latter did not cross the MIZ edge perpendicularly (Figure 3.5b).

Overall, the observed PM products did compare well with ship-based SIC observations (Table 3.1 and Figure 3.8). This was in agreement with Worby and Comiso (2004) who confirmed that the average error of ASPeCt SIC observations relative to satellite data was 10% in total and partial SIC conditions. Although these PM products were reliable, limitations of comparing the two methods were identified. For example, the PM SIC data were an average over two daily swaths, whereas the ship-based data was instantaneous (conducted at an exact time rather than averaged). Therefore, with the current method of retrieving SIC data through PM satellites, it is not possible to uniquely identify the location of the edge and provide a definitive MIZ SIC relationship with *in situ* observations. This limitation is emphasized in winter when the metocean variables are stronger causing rapid changes in the ice edge. Moreover, the relationship observed between ship-based and PM SIC estimates in summer and winter are based on a finite number of samples conducted within a relatively small region in the Atlantic sector. From the finite samples collected within this sector, where ship-based SIC observations have never been collected before, the results presented in Section 3.1 are, therefore, estimations of the relationship between PM and *in situ* SIC recoveries. Many

more expeditions providing an increased number of observations are required to increase the statistical validity of these results.

An additional shortcoming of the relationships presented in Section 3.1 is that neither the uncertainties of the ship-based observations nor the limitations linked to PM SIC measurements can be estimated from the data. Therefore, even if the satellite data would have no error, they would not be expected to correlate perfectly with *in situ* observations because of uncertainties inherent in their collection methodology.

For example, a notable limitation when analysing ship-based observations is the interpretation of the sea ice environment between several inexperienced sea ice observers. This inexperience is due to the observers' lack of exposure to sea ice conditions while living in Africa. This limitation is reinforced by the relative lack of glaciology in the secondary and tertiary education syllabus that could slow down the growth of sea ice science in South Africa. This can result in highly subjective interpretations (thus agreeing with Beitsch et al. (2015), de Jong (2016), and Wagner and Pena (2016)). Even though the sea ice observers have been inexperienced, through regular training programmes, we have developed new skills for South African Polar research (since the first *S.A. Agulhas II* MIZ expedition in winter 2016) which is expected to grow each year.

To increase our understanding on the Antarctic MIZ environment, longer expeditions are needed. Taking into account that the same sea ice observers would not participate every year, a programme of training that would ensure observational continuity is important, as well as the need for an automatic system to retrieve SIC.

4.2 Automatic Acquisition of SIC

There have been several attempts at building an automatic system to retrieve sea ice characteristics. For example, Weissling et al. (2009) automatically calculates frequency distribution of ice floe sizes to compliment ASPeCt observations. Alberello et al. (2019) developed an algorithm to automatically detect floes to extract metrics such as diameter and area within the pancake ice field. Additionally, automatic measurement of pancake size distribution from aerial image stills has been accomplished by Parmiggiani et al.

(2018). Based on the ship-based SIC observation limitations discussed in the preceding section, it is suggested that automatically acquiring SIC from image stills and videos will aid in a sustainable approach to retrieve SIC (see Sections 2.4 and 3.2).

The automatic acquisition method was used during the winter 2017 and summer 2016 *S.A. Agulhas II* expeditions. There was a lower correlation between the automatic acquisition technique and the ship-based observations in winter relative to summer (Figure 3.9). We inferred that the correlation was poor in winter due to liquid on the surface of the ice which could be a result of flooding, melting, or lack of cohesion due to waves. This liquid was predominantly observed during the winter expeditions (Figure 3.6) relative to the summer expeditions (Figures 3.3 and 3.4). Figure 4.1 shows an example of liquid on the surface of the ice causing the threshold method to interpret the centre of the pancake ice as water. When acquiring sea ice features, there may be a marked difference between the primary (the thickest ice present) and the secondary (the second thickest ice present) ice concentration. Alberello et al. (2019) automatically identified the pancake ice from the background water and frazil ice. Our threshold method defined thin ice, such as frazil and brash ice, as water (Figure 4.1). The frazil and brash ice is the secondary ice located in the interstices of the pancakes (the primary ice).

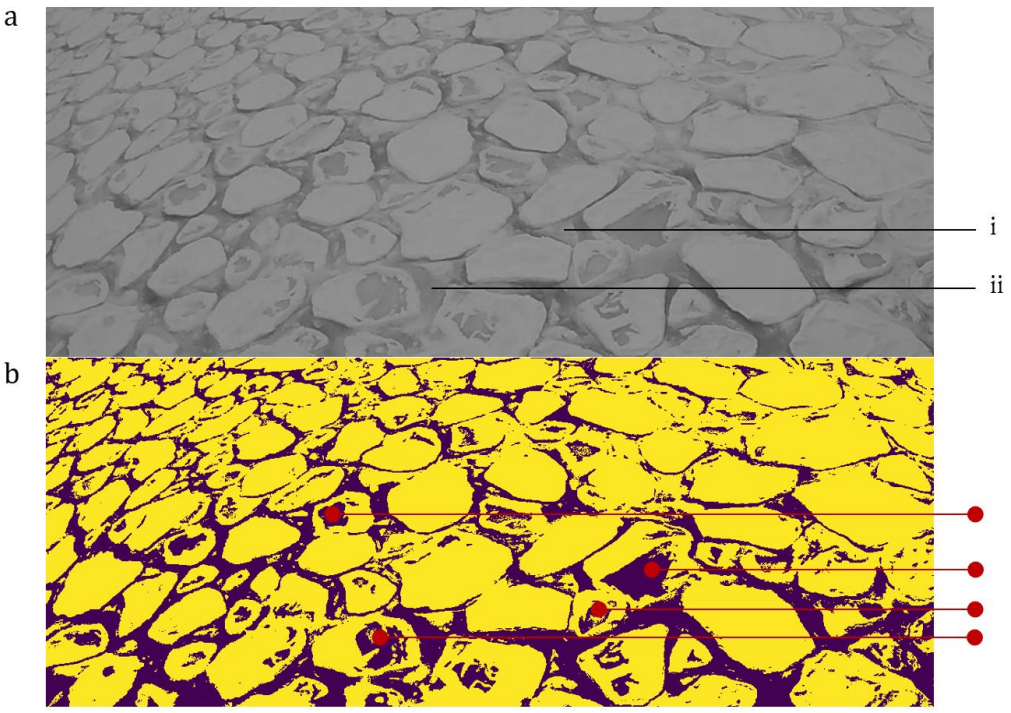

Figure 4.1: Sub-scene image stills depicted in (a) grey scale and (b) binary after using the threshold method: yellow and purple are ice and water, respectively. In the interstices of the pancakes are (i) brash and (ii) frazil ice. A few surface melt signatures in the centre of the pancakes are denoted in red.

In addition to the limitations pertaining to this algorithm i.e. misinterpreting thin ice (brash and frazil ice) and surface liquid as water, this method was further limited by geometric distortion increasing with distance from the ship (Figures 2.10 and 2.11a). However, this geometric distortion did not have a major effect on the results presented in this study because the ship-based observers had the same distortion. For future SIC calculations using this automatic system, orthorectification of the sub-scenes will be necessary (e.g., Weissling et al., 2009) and compared against uncorrected sub-scenes. An in-depth discussion of correcting for the distortion in image stills is provided by Weissling et al. (2009). Figure 4.2 shows an example of an orthorectified image of the sub-scenes presented in Figure 4.1.

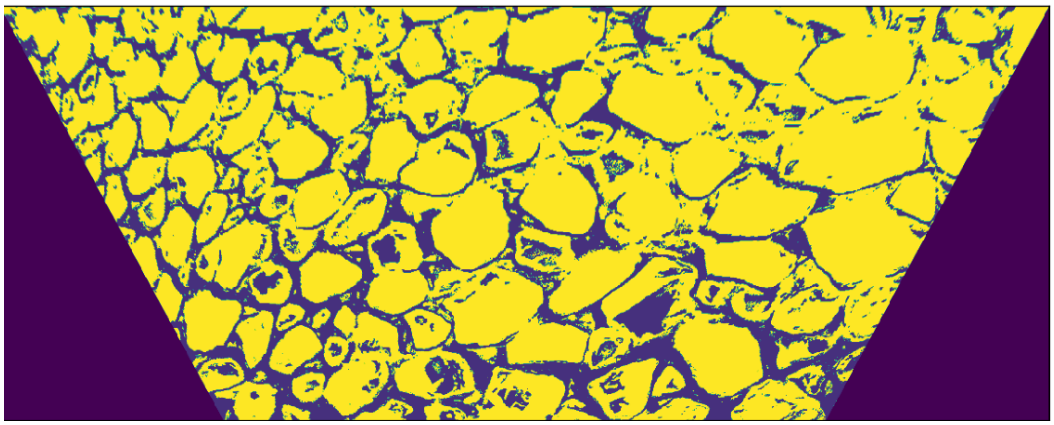

Figure 4.2: Orthorectified image of the subscenes presented in Figure 4.1.

Furthermore, using this method of automatically acquiring SIC may have been impacted by erroneous measurements. For example, a single floe in open water can potentially fill the entire sub-scene, returning 100% SIC rather than the concentration corresponding to the area of study observed using human estimates. To avoid this, a moving average can be included in the algorithm for future calculations. By averaging the data, the spatial resolution of the video data is reduced and, therefore, the data are more comparable to satellite-derived SIC (e.g., Weissling et al., 2009). During future Antarctic expeditions, moving average estimations will be implemented using multiple cameras placed on different sides of the ship. This will allow for increased sea ice coverage.

It is important to note that this algorithm used to automatically acquire SIC does not directly solve the problem of subjective bias. It rather limits the variability of the bias to that of only the people who developed the algorithm. Although the variability is relatively limited, there are still shortcomings linked to this method.

4.3 Seasonal MIZ SIE Observed through Satellite

A methodology fashioned for ship-based sea ice observations aboard the *S.A. Agulhas II* was provided in Section 2.1. Using these ship-based SIC observations, the data obtained with AMSR2 estimates was assessed (Section 3.1). This assessment was the first step towards quantifying the uncertainties when using PM-SIC datasets within the MIZ

in the Atlantic sector. Having in mind the limitations of satellite measurements in the MIZ, in Section 3.3 we presented an analysis of how the variability in MIZ extent relates to the total SIE within the Atlantic.

In the studied cases, the MIZ edge estimation based on different satellite algorithms was approximately 13 km (Section 4.1). Therefore, the ASI-SSMIS product with a 12.5 km grid-resolution (see Section 2.2.1) can reliably be used when undertaking climatological studies during winter in the Atlantic. Globally, the seasonal sea ice variability includes retreating extent in summer and growth in winter, where the minimum and maximum SIE is reached in February and September, respectively (Figures 1.1 and 3.10). This seasonal pattern remains the same within the Atlantic sector (see Figure 3.12). As found in other regions, the seasonal variability differs from year to year, resulting in some years possessing anomalously high or low SIE relative to the climatology. As summarised by Maksym (2018), 2016 and 2017 were two record-low anomalous years (Figure 3.11a), erasing the statistical significance of previously reported increasing Antarctic SIE trends. We suggested that these Southern Ocean anomalies may have happened from the month of September 2016 and remaining at low levels through 2017 (Figure 3.11b). Turner et al. (2017) found that the 2016 anomalous decrease happened over spring (September – November), observing that this Antarctic anomalous retreat caused the SIE to remain at low levels until March 2017.

Through observing regional heterogeneity within the Atlantic sector, we found that, although the September 2016 and 2017 extent was anomalously lower over the Southern Ocean, the September 2016 Atlantic sector SIE was noticeably higher than the climatology (whereas the September 2017 SIE was still lower relative to the climatology within this region) (Figure 3.12). In addition to the anomalously high 2016 SIE in September, the SIE rapidly retreated from November through to December 2016 within the Atlantic sector (Figure 3.12). These results were similar to Turner et al. (2017) who found that the Weddell Sea showed record low SIE anomalies from November 2016 to early April 2017.

Focussing on this spring SIE variability, it was found that these recorded anomalous patterns were highlighted within the MIZ (Figure 3.13). Therefore, we investigated the seasonal variability of the MIZ extent with respect to the total SIE. As expected, on average, the extent of the MIZ gradually increases throughout the year (Figure 3.14i). Figure 3.14 shows that while the total SIE starts to retreat in September, the MIZ, in turn, expands further north. Similar MIZ trends have been studied as annual means by Stroeve et al. (2016) but, to our knowledge, the seasonal variation and its relationship with the total SIE has not been investigated. By calculating the ratio of the MIZ extent to the total SIE over the Eastern Weddell, Lazarav, and Riiser-Larsen sectors (Figure 3.14ii), we noticed that the MIZ in mid-winter to early-spring (July – September) may act as an indicator of how the evolution of SIE may be manifested over the months to follow (October – December). If this is the case, we predict from Figure 3.14 that when the MIZ extent increases in relation to the climatology, it is more likely that total SIE will decline over the following months. We additionally observed that once the total SIE begins to decline in spring (September – November), it will continue to retreat at a relatively fast rate until early-February. As seen in Figures 3.14a and 3.14b, this was observed in the Eastern Weddell and Lazarev sectors, respectively. For example, within these sectors during 2016, there was, on average, a sudden rise in MIZ extent in August and September, followed by a sudden decline in total SIE in October. Within the Lazarev sector in 2017, there was a rise in MIZ extent from July – September and a steep decline in total SIE over the following months. The connection between the MIZ SIE and total SIE is elucidated through observing their ratio in Figure 3.14ii where we observe that 2016 and 2017 had, on average, a higher ratio with respect to the climatology from August onwards.

Therefore, to predict what the total SIE will look like over the spring to early-summer months (September – December), we suggest observing the ratio between the MIZ SIE and total SIE. This suggested link was further supported when, in Figure 3.14, we included the year 2015 (a year with seasonal variability similar to that of the Atlantic sector's climatology (Figure 3.12)). We suggest that if the ratio of the MIZ extent and the total SIE of a particular year remains within one standard deviation of the climatology

during the autumn and early-spring months (April – September), this year will not show anomalous seasonal variability in the months to follow.

It is important to note that using the MIZ as an indicator for the evolution of the following months is speculation based on the analysis of a few years. The observed link between total and MIZ extent needs to be confirmed by analysing longer data sets of preceding years.

4.4 Conclusions

Although one of the biggest seasonal changes on Earth is the annual advance and retreat of the Antarctic sea ice cover, relatively little attention has been given to the processes by which the MIZ edge forms and responds to synoptic events. This study aimed to assess the seasonal cycle of the MIZ extent by comparing sea ice observations estimated from aboard ship to high resolution PM satellite imagery. From comparing SIC derived from satellites and ship-based observations, we were able to suggest that PM products are limited when estimating ice concentration in winter. However, the limitations suggested in this study are specific only to regions within the east Atlantic sector. By comparing the ship-based ice concentration results to high-resolution PM-SIC estimates, it was observed that deriving sea ice features, through using these satellite products, was more uncertain during winter MIZ conditions. Since the Antarctic MIZ is largely influenced by metocean variables in winter (i.e. the strongest wind and waves on Earth) relative to summer, we suggested that such metocean variables may cause a disturbance in the sea ice environment, affecting the heterogeneity of the sea ice surface which may weaken the quality of the PM ice concentration measurements in winter. When strong wind and waves cause water to flood the surface of the ice, surface liquid may appear as a mixture of ice and open water to the PM sensors. Additionally, thin ice such as frazil and brash may also be interpreted as open water. Local, ship-based validation plays a complementary role in helping to interpret ice concentration derived from satellites by highlighting shortcomings inherent in satellite SIC imagery. To better understand the variability of the Antarctic sea ice, it is necessary to acquire as many direct observations

as possible to validate the satellite methods and to quantify regional characteristics. Therefore, the continuation of ship-based collections from all ships sailing through Southern Ocean sea ice should be ensured. Furthermore, in future studies, SIC derived from ship-based observations should be validated against satellite products monitoring the MIZ at higher resolutions. In particular, satellite products such as MODIS (Moderate Resolution Imaging Spectroradiometer) (e.g. Zhao et al., 2017) and GNSS-R (Global Navigation Satellite Systems-Reflectometry) (e.g. Arroyo et al., 2017).

To accomplish this local SIC validation, a proper protocol of ship-based field programmes must be maintained on South African ships, while, in parallel, recognizing the shortcoming linked to such programmes. For example, the ship-based ice concentration observations collected for this study were linked with their own errors such as subjective bias of human interpretation and lack of expertise. These errors may be reduced or assessed by the development of an algorithm to automatically acquire ice concentration from image stills and videos. This method can be used to obtain quantitative sea ice data from vessels of opportunity without the need to have trained personnel on-board.

From the *in situ* and satellite comparison results, an analysis of the seasonal extent was accomplished while being aware of the winter limitations inherent in PM products. Having in mind the limitations of satellite measurements in the MIZ, in Section 3.3 we presented an analysis of how the variability in MIZ extent relates to the total SIE within the Atlantic. From these results, it was suggested that the seasonal cycle of the MIZ extent is different to the variability of the total extent. Through observing the ratio between these extents, we inferred that the mid-winter to early-spring MIZ extent may act as an indicator of how the evolution of the total ice extent may be manifested over the months to follow. We therefore suggest that understanding the variability of the winter MIZ is required for projecting the spring and summer total ice extent. Since intense ice-ocean-atmosphere interactions take place within the MIZ, we agree with Stroeve et al. (2016) who suggested that an expanding or retreating MIZ may help to shed light on the metocean processes impacting the observed trends in total extent.

List of References

Alberello, A., Onorato, M., Bennetts, L., Vichi, M., Eayrs, C., MacHutchon, K., and Toffoli, A. 2019. Brief communication: Pancake ice floe size distribution during the winter expansion of the Antarctic marginal ice zone. *The Cryosphere*, 13:41-48.

Alonso-Arroyo, A., Zavorotny, V.U., and Camps, A. 2017. Sea Ice Detection Using U.K. TDS-1 GNSS-R Data. *IEEE,* PP(99):1-13.

Antarctic Sea-Ice Processes and Climate (ASPeCt), (Online). Available at: http://aspect.antarctica.gov.au/ (Accessed 21 August 2017).

Antarctic Sea-Ice Processes and Climate (ASPeCt). 1998-2008. *Science and Implementation Plan*, (Online).Available: http://aspect.antarctica.gov.au/__data/assets/pdf_file/0005/59126/ASPECT_SciImplPlan.pdf (Accessed: April. 14, 2017).

Bietsch, A., Kern, S., and Kaleschke, L. 2015. Comparison of SSM/I and AMSR-E Sea Ice Concentrations With ASPeCt Ship Observations Around Antarctica. *IEEE Transactions on Geoscience and Remote Sensing,* 53(4):1985-1996.

Cavalieri, D.J., Markus, T., Hall, D.K., Ivanoff, A., and Glick, E. 2010. Assessment of AMSR-E Antarctic Winter Sea-Ice Concentrations Using Aqua MODIS. *IEEE Transactions on Geoscience and Remote Sensing,* 48(9):3331-3339.

Collins III, C.O., Rogers, W.E., Marchenko, A., and Babanin, A.V. 2015. In situ measurements of an energetic wave event in the Arctic marginal ice zone. *Geophysical Research Letters,* 42:1-8.

Comiso, J.C. 2006. Abrupt decline in Arctic winter sea ice cover. *Geophysics Research Letters*, 33:1-5.

Comiso, J.C. 1995. SSM/I Sea Ice Concentrations Using the Bootstrap Algorithm. *NASA Ref. Publication 1380,* (Online). Available: https://www.geobotany.uaf.edu/library/pubs/ComisoJC1995_nasa_1380_53.pdf. (Accessed: February 05, 2018).

Comiso, J.C., Kwok, R., Martin, S., and Gordon, A.L. 2011. Variability and trends in sea ice extent and ice production in the Ross Sea. *Journal of Geophysics Research,* 116:1-19.

Davies, B. 2015. Increasing Antarctic Sea Ice. *AntarcticGlaciers.org,* (Online). Available at: http://www.antarcticglaciers.org/glaciers-and-climate/ice-ocean-interactions/antarctic-sea-ice/. (Accessed: May 04, 2017).

de Jong, E. 2016. *Antarctic 2012 and 2015 Winter Sea Ice Concentration within the Marginal Ice Zone: Comparison of in situ ASPeCt observations and satellite passive microwave estimates.* Honours thesis, University of Cape Town.

Dieckmann, G.S., and Hellmer, H.H. 2010. Sea Ice. The Importance of Sea Ice: An Overview, 2nd ed. Wiley-Blackwell, pp. 1-22.

Doble, M.J., De Carolis, G., Meylan, M.H., Bidlot, J., and Wadhams, P. 2015. Relating wave attenuation to pancake ice thickness, field measurements and model results. *Geophysical Research Letters,* 42:4473-4418.

Doble, M.J., and Wadhams, P. 2006. Dynamical contrasts between pancake and pack ice, investigated with a drifting buoy array. *Journal of Geophysical Research*, 111:1-11.

Doble, M.J. Wadhams, P., and Coon, M.D. 2003. Pancake ice formation in the Weddell Sea. *Journal of Geophysical Research*, 108(C7):3209.

Heygster, G., Wiebe, H., Spreen, G., and Kaleschke, L. 2009. AMSR-E Geolocation and Validation of Sea Ice Concentrations Base on 89 GHz Data. *Journal of Remote Sensing Society of Japan,* 29:226-235.

Ivanova, N., Pedersen, L.T., Tonboe, R.T., Kern, S., Heygster, G., et al. 2015. Inter-comparison and evaluation of sea ice algorithms: towards further identification of challenges and optimal approach using passive microwave observations. *The Cryosphere,* 9:1797-1817.

Kaleschke, L.C., Lüpkes, C.. Vihma, T., Haarpainter, J., Bochert, A. et al. 2001a. SSM/I Sea Ice Remote Sensing for Mesoscale Ocean-Atmosphere Interaction Analysis. *Canadian Journal of Remote Sensing*, 27(5):526-537.

Kaleschke, L., Girard-Ardhuin, F., Spreen, G., Beitsch, A., and Kern, S. 2001b. ASI Algorithm SSMI-SSMIS sea ice concentration data, originally computed at and provided by IFREMER, Brest, France, were obtained as 5-day median-filtered and gap-filled product for (1997-2017) from the Integrated Climate Date Center (ICDC, icdc.cen.uni-hamburg.de/), University of Hamburg, Hamburg, Germany.

Kohout, A.L., Williams, M.J.M., Dean, S.M., and Meylan, M.H. 2014. Storm-induced sea-ice breakup and the implications for sea ice extent. *Nature*, 509:604-607.

Maksym, T. 2018. Arctic and Antarctic Sea Ice Change: Contrasts, Commonalities, and Causes. *Annual Review of Marine Science.,* 11: 19.1-19.27.

Martinson, D.G. 2012. Antarctic circumpolar current's role in the Antarctic ice system: An overview. *Palaeogeography, Palaeoclimatology, Palaeoecology,* 335-336:71-74.

Mateur, R.J., O'Kane, T.J., Risbey, J.S., and Chamberlain, M. 2015. Sources of heterogeneous variability and trends in Antarctic sea-ice. *Nature Communications,* 6:1-9.

Meier, W.N. and Stroeve, J. 2008. Comparison of sea-ice extent and ice-edge location estimates from passive microwave and enhanced-resolution scatterometer data. *Annals of Glaciology,* 48:65-70.

Pang, X., Pu, J., Zhao, X., Ji, Q., Qu, M., and Cheng, Z. 2018. Comparison between AMSR2 Sea Ice Concentration Products and Pseudo-Ship Observations of the Arctic and Antarctic Sea Ice Edge on Cloud-Free Days. *Remote Sensing,* 10:1-13.

Parmiggiani, F., Moctezuma-Flores, M., Wadhams, P., and Aulicino, G. 2018. Image processing for pancake ice detection and size distribution comparison. *International Journal of Remote Sensing,* doi: 10.1080/01431161.2018.1541367.

Petty, A.A., Stroeve, J.C., Holland, P.R., Boisvert, L.N., Bliss, A.C., et al. 2018. The Arctc sea ice cover of 2016: a year of record-low highs and higher-than-expected lows. *The Cryosphere,* 12:433-452.

Petrich, C and Eicken, H. 2010. *Sea Ice: Growth, Structure and Properties of Sea Ice*. 2nd ed. Wiley-Blackwell. pp. 23-78.

Spreen, G., Kaleschke, L., and Heygster, G. 2008. Sea ice remote sensing using AMSR-E 89-GHz channels. *Journal of Geophysical Research*, 113:1-14.

Stammerjohn, S., Massom, R., Rind, D., and Martinson, D. 2012. Regions of rapid sea ice change: An inter-hemispheric seasonal comparison. *Geophysical Research Letters,* 39:1-8.

Soal, K., Bienert, J., and Bekker, A. 2005. Operational Model Analysis on the Polar Supply and Research Vessel the S.A. Aguhas II. *International Operational Model Analysis Conference (IOMAC'15).*

Stroeve, J.C., Jenouvrier, S., Campbell, G.G., Barbraud, C., and Delord, K. 2016. Mapping and assessing variability in the Antarctic marginal ice zone, pack ice and coastl polynyas in two sea ice algorithms with implications on breeding success of snow petrels. *The Cryosphere*, 10:1823 – 1843.

Taylor, K.E. 2001. Summarizing multiple aspets of model performance in a single diagram. *Journal of Geophysical Research,* 106:7183-7192.

Turner, J., Hosking, J.S., Marshall, G.J., Phillips, T., and Bracegirdle, T.K. 2016. Antarctic sea ice increase consistent with intrinsic variability of the Amundsen Sea Low. *Climate Dynamics,* 46:2391-2402.

Turner, J., Phillips, T., Marshall, G.J., Hosking, J.S., Pope, J.O., Bracegirdle, T.J., and Deb, P. 2017. Unprecedented springtime retreat of Antarctic sea ice in 2016. *Geophysical Research Letters,* 44:6868-6875.

Wadhams, P., Parmiggiani, F.F., de Carolis, G., Desiderio, D., and Doble, M.J. 2004. SAR imaging of wave dispersion in Antarctic pancake ice and its use in measuring ice thickness. *Geophysical Research Letters,* 31:1-5.

Wadhams, P., Squire, V.A., Ewing, J.A., and Pascal, R.W. 1986. The Effect of the Marginal Ice Zone on the Directional Wave Spectrum of the Ocean. *Journal of Physical Oceanography*, 16:358-376.

Wagner, P., and Pena, J. 2016. Ice Observations. (Online) Available at: http://www.utsa.edu/lrsg/antarctica/simba/projects/simba_final_ice_observations.doc. (Accessed: 29 August 2016).

Weeks**,** W.E., and Ackley, S.F. 1986. The growth, structure, and properties of sea ice. *Geophysics of Sea Ice,* 146:9-164.

Weissling, B., Ackley, S., Wagner, P., Xie, H. 2009. EISCAM – Digital image acquisition and processing for sea ice parameters from ships. *Cold Regions Science Technology,* 57:49-60.

Worby, A.P., and Allison, I. 1999. Cooperative research centre for the Antarctic and Southern Ocean environment: A Technique for Making Ship-Based Observations of Antarctic Sea Ice Thickness and Characteristics; Part I: Observational Technique and Results. *Antarctic CRCI*, 14:6-23.

Worby, A.P., and Comiso, J.C. 2004. Studies of the Antarctic sea ice edge and ice extent from satellite and ship observations. *Remote Sensing and Environment*, 92:98-111.

World Meteorological Organisation (WMO). 2009. *WMO Sea-Ice Nomenclature*. 07 October 2009. (Online). Available at: https://www.jcomm.info/index.php?option=com_oe&task=viewDocumentRecord&docID=4438 (Accessed 15 January 2019)

Zhao, X., Su, H., Stein, A., and Pang, X. 2017. Comparison between AMSR- ASI sea-ice concentration product, MODIS and pseudo-ship observations of the Antarctic sea-ice ridge. *Annals of glaciology,* 56(69):45-52.